L.N.L.-I.N.F.N. (REP) 197/2003

Istituto Nazionale
di Fisica Nucleare
Laboratori Nazionali di Legnaro

Preliminary design and beam dynamics simulations of the EURISOL linac post-accelerator

Dan Berkovits[1] and Alberto Facco
Berkovits@lnl.infn.it, Facco@lnl.infn.it.
LNL-INFN

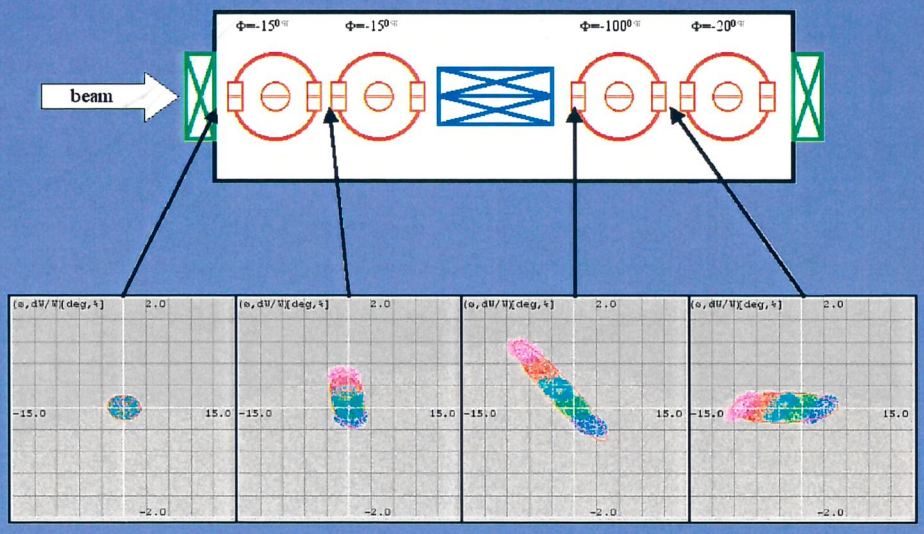

November 2002

On leave from SOREQ NRC, Yavne 81800, Israel, berkova@soreq.gov.il

L.N.L.-I.N.F.N. (REP) 197/2003

Preliminary design and beam dynamics simulations of the EURISOL linac post-accelerator

Dan Berkovits[1] and Alberto Facco
Berkovits@lnl.infn.it, Facco@lnl.infn.it

LNL-INFN

November 2002

[1] On leave from SOREQ NRC, Yavne 81800, Israel, berkova@soreq.gov.il

Index

1 Introduction

The EURISOL [1] post-accelerator is designated to accelerate all radioactive ions, produced in an ISOL target and delivered by a charge breeder, to any specified final energy up to a value of 100 MeV/u, with fine energy tunability at least up to 10 MeV/u [2]. The difficulty of producing radioactive ions in sufficient numbers, together with the unavoidable losses during extraction and charge breeding, requires a post-accelerator able to preserve as much as possible the beam intensity. Good beam quality (low emittance) is also required for most of the planned nuclear physics experiments, at least near or below the Coulomb barrier energy. The EURISOL post-accelerator, moreover, must have a competitive construction and operation cost.

In this paper we propose a solution based on linac technologies that, in comparison with other proposed solutions based on cyclotron accelerators [3], could present significant advantages in terms of efficiency, flexibility, performance and cost.

Superconducting (SC) linacs with independently phased cavities, widely used for two decades in many laboratories for all kinds of stable ions, are very well suited to the EURISOL post-accelerator requirements [4,5] due also to two recent achievements in the field of superconducting linacs:

1. The possibility of producing (at a reasonable cost) high-gradient low-beta cavities: the average gradient obtained by the latest generation of cavities in off-line testing is near 7 MV/m at 7 W: this value could be considered a realistic design gradient for a future linac [6].
2. The multi-charge beam transport, first suggested and demonstrated at ANL by Ostroumov *et al.* [7,8] and today a basic ingredient of the American proposal RIA (Rare Ion Accelerator). This technique allows efficient transmission after intermediate stripping.

A SC linac based on presently available high-gradient cavities, like the quarter wave resonator (QWR) of ALPI at Legnaro, can therefore be built at a considerably lower cost than the one required only a decade ago. The design of such a post-accelerator for EURISOL, however, introduces a new beam dynamics challenge, i.e. the control of the beam steering of highly charged beams caused by the asymmetric QWR electromagnetic

field. This effect is negligible in the existing heavy ion SC linacs with low q/A ions and/or low accelerating gradient. For the EURISOL post-accelerator case, on the contrary, this effect is very pronounced and can be critical. The QWR magnetic steering problem was first pointed out and studied at LNL [9] in the beginning of 2001; corrections of this phenomenon by cavity modification and beam optics compensation have been proposed at ANL [10], LNL [11] and IKF Juelich [12] during the same year.
New problems in beam dynamics, introduced by the need of handling very low intensity radioactive beams, encouraged the development of beam dynamics simulation codes. The LANA code of Michigan State University [13], that we have used in our study, was upgraded by including real field distribution, QWR steering effects, stripping sections and multi-charge beam transport. Such a code has become available to us since September 2001 [14].

The current document summarizes the main ideas and beam dynamics simulation that we have produced for the EURISOL post-accelerator between September 2001 and June 2002. This is only a preliminary study, which would require further optimisation and refinement before reaching a construction design; the main aim of this work, however, has been to demonstrate the feasibility of the scheme and to calculate the main characteristics and performance of the linac.
The EURISOL committee advised, for the benchmark calculation, a reference beam of ^{132}Sn delivered by a charge breeder in a charge state 25+ at the energy of 2.35 keV/u. The full post-accelerator linac proposed for EURISOL is described elsewhere [4,5]; the current document summarizes the beam dynamics simulation of the linac section which starts at 670 keV/u, downstream three SC RFQs, and ends at 100 MeV/u for the nominal beam.

This study includes:

1. Optimisation of the stripping stations location.
2. Verification of multi-charge beam transport through the linac and transmission efficiency maximization.
3. 3-dimensional beam dynamics simulation with real field distribution in cavities (calculated with the code HFSS).
4. Study of the QWR beam steering effect in different linac lattices in order to check the possibility of using existing QW resonators without major modifications.

The simulation work started in October 2001 and was performed during three time periods; the first iteration was completed for the second EURISOL town meeting held in Abano Terme in January 2002. The second iteration lead to a refinement of the first simulation in a few weak points, and ended for the EPAC2002 meeting held in Paris in June 2002. The third iteration, after EPAC2002, added only small corrections. This document is written following this time evolution.

2 The beam dynamics simulation challenge

Beam dynamics studies and simulation of multi-charge beam transport in superconducting linacs have been performed at ANL [15] and MSU [16,17,18] for the RIA driver accelerator, and at TRIUMF for the ISAC-II post-accelerator [19,20,21]. The relevant concepts and results of these studies, reflected in their publications (and in fruitful discussions we had with Matteo Pasini from TRIUMF and Dmitry Gorelov from MSU along the year), have been taken into account also in the present work. Together with many similarities, however, there are several substantial differences among all these projects:

1. For the RIA driver accelerator, due to its rather high beam current, the main concern regarding the beam emittance is its influence to the beam losses; energy spread of 10 % and bunch size of 70 deg are accepted if they do not produce damaging or activation of the linac. For the EURISOL post-accelerator, characterised by very low beam current, the beam quality specifications are dictated mainly the nuclear physics experiments requiring energy spread less than 0.1 % and time spread less than 500 ps [22]. These tough demands require a

careful study of the effects of strippers in the post-accelerator, which are the main source of emittance growth; the results of our work in this subject have been published elsewhere [23] and the beam dynamics simulation presented in this document include these effects.

2. The low current of the EURISOL post-accelerator allows strong beam focusing and bunching on the strippers; this allows to keep emittance growth small. This is not possible in the RIA driver, where the high beam current would cause an unacceptable damaging of the stripper (for this reason new stripper technologies are under development). This prompted us to develop a special beam bunching section in front of each stripper.
3. The low beam current at the post-accelerator (and hence the low beam power loss) allows us to use superconducting RFQs as injectors to the SC linac [24]. The RIA driver includes a normal-conducting RFQ [25] that is planned to transport two charge states simultaneously. Many, but not all, of the initial parameters for the design of the Eurisol Superconducting Reaccelerator Linac (SRL from now on) are driven by the RFQ characteristics. The initial parameters for SRL, compared to the RIA driver ones, are shown in table 1.
4. The optimisation of the strippers locations depends on the final energy and reference particle choice. For SRL (RIA driver) the reference particle is ^{132}Sn (^{238}U) and the final energy is 100 (400) MeV/u. The best location for the first stripper was found to be at 4.3 MeV/u (9.4 ANL [15] and 13.5 MSU [16]), and at 22.4 (85) MeV/u for the second one. An important parameter is the width of the mass to charge ratio distribution after stripping. After the first foil, the 5 more populated charge states that must be accelerated have a total $\Delta q/q$ (half width) =6.6 % in SRL, and 3.5 % in the RIA driver. This large $\Delta q/q$ requires a careful adjustment of the synchronous phases for each different charge states.
5. The cavities bore diameter in the ANL [15] and MSU [14] driver accelerator design is 3 cm, while in SRL it is only 2 cm. This difference has a moderate influence in the cavity real field distribution and performances. The smaller aperture decreases the transversal acceptance of the linac and requires a different focusing power along the accelerator.

6. The last important difference between the RIA driver and SRL is the fact that the latter needs a stable pilot beam in order to tune the accelerator. The very weak signal from the beam diagnostics devices along the linac, due to the very low current of most radioactive beams, would make this operation extremely difficult and time consuming in SRL. The linac design should take this into account (this subject, however, is not included in this paper). For example, the natural pilot beam for the reference ^{132}Sn beam is its stable isobar ^{132}Xe. The 4 atomic number difference between the two isobars creates a large difference in the charge state population after the (second) stripper. The chosen reference charge state for the beam dynamics calculation and tuning should be populated by both isobars.

The ISAC-II post-accelerator has many similarities with SRL, since it is using the same type of resonators developed at LNL. However this linac, under construction, is based on well-established technologies and performance (acceleration gradient, charge breeder), while the EURISOL design includes future technological developments. The initial beam parameters (table 1) and the final maximum output energy (10 MeV/u) of ISAC-II require the first stripper at a much lower energy (0.4 MeV/u) than in SRL. In addition, ISAC-II is limited to the real-estate space available at TRIUMF, while in SRL and RIA this is a free parameter.

Table 1: Initial beam parameters, at the RFQ exit, for the beam dynamics simulation of the EURISOL post-accelerator (SRL) and for other multi-charge beam transport studies.

	SRL [5]	ISAC-II [20]	RIA driver[1]	
			ANL [15]	MSU [18]
Reference particle	^{132}Sn	^{132}Sn	^{238}U	
Current	≤1 nA		4.2 pμA	
Energy (keV/u)	670	150	170	295
Longitudinal emittance (π keV/u ns)	0.5	0.6	2.3	1.2
Norm. transverse emittance (π mm mrad)	0.6	0.1		0.6
Bunch frequency (MHz)	80	35	57.5	80.5
Mass to charge ratio (a.m.u./e)	5.3	7	8.3	

(1) Acceleration of two charge states, 28+ and 29+, simultaneously through the RFQ

In the following sections the conceptual design scheme of SRL, based on the reference beam ^{132}Sn, will be described. This design, however, would have similar or higher efficiency for nearly all of the radioactive beams foreseen in EURISOL.

3 The EURISOL post-accelerator layout

A schematic layout of SRL is shown in figure 1. A radioactive beam with A/q≤10 (up to $^{132}Sn^{13+}$) is delivered by the charge breeder at 2.3 keV/u, and then injected in a 4 m long section consisting of 3 superconducting RFQs housed in 2 cryostats. This section resembles the LNL-PIAVE design, with the addition of one bunching RFQ; the beam is bunched at 80 MHz and accelerated to 670 keV/u with 95 % transmission. The normalized rms emittance, calculated at the RFQ exit, is 0.1 (π mm mrad) and 0.1 (π keV/u ns) [24].

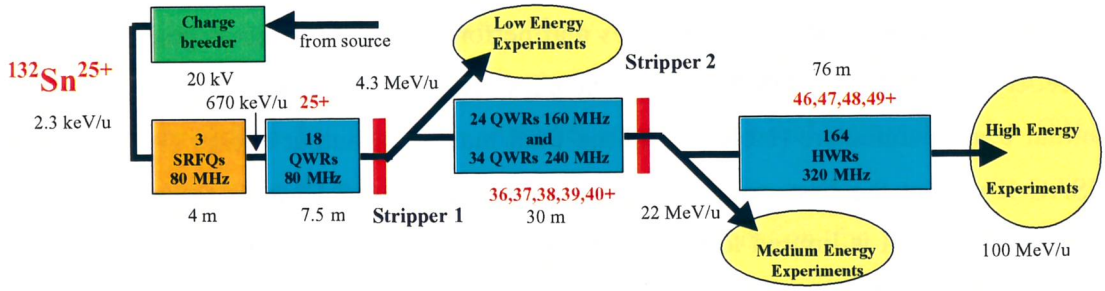

Fig 1: Schematic layout of the proposed superconducting post-accelerator linac with two intermediate stripping stations. The energy and charge state values are referred to the test case beam, ^{132}Sn.

The RFQs are followed by the Independently-phased Superconducting Cavity Linac which is the subject of this paper. It includes three sections, low energy (LE), medium energy (ME) and high-energy (HE), each optimised for different velocity and charge to mass ratio (q/A) (figures 1, 2 and table 2). The superconducting resonators are of the Quarter-Wave and Half-Wave (HWR) type, with rf frequency from 80 to 320 MHz and different values of optimum velocity β_0; these 2-gap cavities are characterized by large velocity acceptance and high accelerating gradient. The basic linac module consists of cryostats containing 4 or 8 resonators and one superconducting solenoid in the center (figures 3, 4 and table 3). This configuration allows a rather compact design.

A 40 cm gap between two cryostats is reserved for vacuum bellows and beam diagnostics devices, which are thus located in a beam waist position. Each cavity is operated at 7 MV/m accelerating field, with 10 W power dissipation at 4.2 K [6].

Table 2: Superconducting 2-gap resonator parameters used in the SRL beam dynamics simulation.

Energy section	Low		Medium		High
Cavity type	QWR	QWR	QWR	QWR	HWR
Frequency (MHz)	80	80	160	240	320
n.	4	14	24	34	164
Optimum velocity β_0	0.047	0.055	0.110	0.165	0.28
Acceleration gradient (MV/m)	7	7	7	7	7
Acceleration gap (cm)	4.0	4.0	4.0	4.0	5.0
Drift tube (cm)	4.0	6.0	6.0	6.0	7.4
Effective length (cm)	18	18	18	18	22.4
Outer diameter (cm)	23.2	23.2	23.2	23.2	28

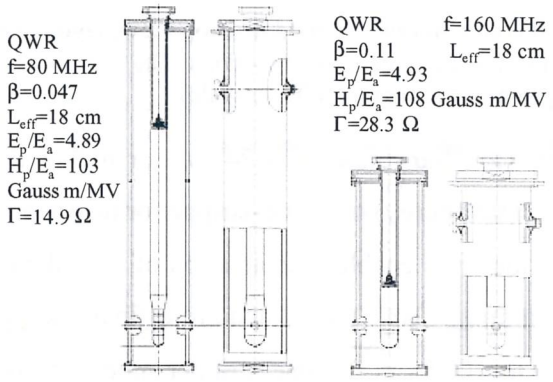

Figure 2: Example of two LNL SC QWR cavities.

The linac layout includes two intermediate stripping stations. Each stripper is followed by a matching section, allowing either injection of the multi-charge beam to the consecutive linac section or beam extraction and charge selection (when required). The multi-charge bending lines used in the present work are the results of theoretical studies done at ANL [26], MSU [27] and TRIUMF [28].

The SRL linac is planned for three modes of operation. According to the required beam energy, the beam is extracted at one of the intermediate positions or at the end of the linac; one, two or no strippers can be used. In any of these modes, the final beam energy can be finely tuned to any intermediate value by properly setting the accelerating gradient of the cavities. The nominal design was optimised for the 2-strippers mode of operation with ^{132}Sn ions injected at charge state q=25+; in this case, the final energy is

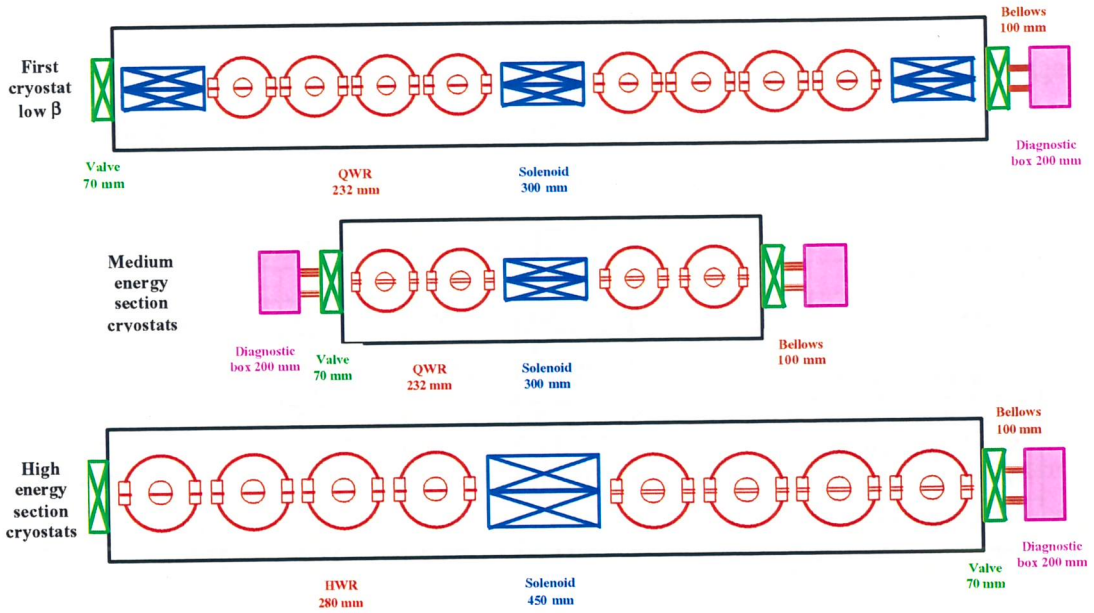

Figure 3: The most common cryostat modules, top view; layout used in the beam dynamics simulation for the three energy sections. The components length along the beam axis is given in the figure (NOT to scale).

100 MeV/u and the total ion transmission is 74 %. For higher transmission and better beam quality (but lower final energy) only one-stripper or no-stripper mode must be used. The large acceptance of the linac enables acceleration of all radioactive beams that allow charge breeding. For example, $^{33}Ar^{8+}$ would acquire a final energy of 130 MeV/u and a total transmission close to 100 % in the one-stripper mode of operation, while $^{210}Fr^{25+}$ would reach 96 MeV/u and a total transmission of 59 % in the 2-stripper mode (see section 4.3).

The strippers make the linac relatively insensitive to the charge breeder performance: with initial charge of 13+, the final energy of the ^{132}Sn beam would be 95 MeV/u without any modification after the RFQ section (see section 4.4).

Table 3: Cryostats parameters and cryostats internal layout. The cryostat length given in the right column is the flange-to-flange distance.

Cryo. number	Qty.	Energy section	First element in cryo	Cavity		Solenoid		Cavities per solenoid	Cryo. length (cm)
				Qty.	f (MHz)	Qty.	Length (cm)		
1	1	LE	Solenoid	8	80	3	30	4	320
2	1	LE	Solenoid	10	80	3	30	5	366
3-8	6	ME	QWR	4	160	1	30	4	157
9-15	7	ME	QWR	4	240	1	30	4	157
16	1	ME	QWR	6	240	1	45	6	218
17	1	HE	Solenoid	4	320	1	45	8	186
18-37	20	HE	HWR	8	320	1	45	8	303

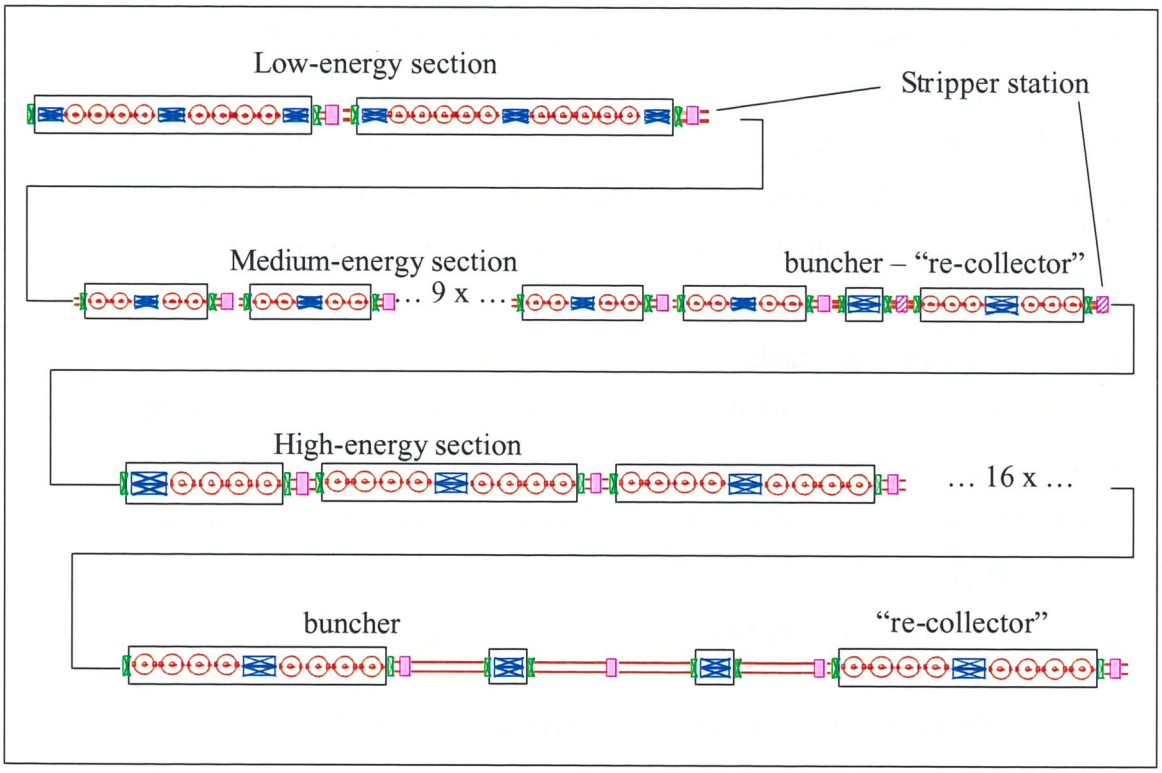

Figure 4: Schematic cryostat distribution along the three ISCL sections.

4 Analytical dynamics

4.1 Energy gain

The ion energy evolution along the linac and the number of cavities of each type (see table 2), as functions of the stripper positions, have been studied and optimised first by means of an analytical approach. Beam dynamics simulation showed from the beginning that convenient locations for the strippers are the ones along the linac where the resonators rf frequency is changed. Multi-charge beam transport, in fact, requires phase synchronization both after each stripper and after each change of frequency (see section 6.1.3.1); locating both changes in one position minimizes the need of matching sections. Higher charge state and higher frequency, on the other hand, cause a sudden increase in the QWR beam steering [9,10,11]. This was found to cause unacceptable emittance growth after the first stripper, which optimum position (3.2 MeV/u; β=0.083) was calculated to maximize the linac energy gain. Since the QWR steering decreases rapidly with β [10,11] the first stripper was moved to 4.3 MeV/u (β=0.096) and emittance degradation became acceptable.

The preliminary study of the longitudinal beam dynamics is based on the on-axis transit time factor (TTF) and energy gain. For this standard calculation a uniform electric field in the resonator gaps is assumed. The TTF for a π-mode one-gap and 2-gap cavities are given by [29]:

$$TTF_1 = \sin(\pi g/\beta\lambda)/(\pi g/\beta\lambda) \qquad \text{for } g \ll \beta\lambda \qquad (1)$$

$$TTF_2 = \sin(\pi d/\beta\lambda)\, TTF_1 \qquad (2)$$

where g is the gap lengths given in table 2, d is the gap to gap distance (centre to centre), λ is the cavity wavelength (that is related to the cavity frequency given in table 2 by $\lambda = c/f$) and assuming a negligible velocity change in the gap.

The energy gain is then given by [29]:

$$\Delta E = q_0 E_a L \; TTF_2(\beta) \cos(\phi) \qquad (3)$$

where L is the resonator effective length, E_a is the acceleration gradient given in table 2 and ϕ is the synchronous phase of the reference charge q_0 (ϕ_{q0}=-20^0 in our case).

4.2 Stripping

The strippers are assumed to be carbon foils, of a thickness sufficient to let the ions reach steady charge state distribution (the choice of this thickness will be explained in section 6.1.2). The charge distribution calculations have been performed using three different formulas. The particle energy used in the calculation is the average energy in the foil (i.e. the incident particle energy minus half of the energy lost in the stripper carbon foil); stripper thickness of 0.2, 2 and 3 mg/cm^2 have been used for the incident ^{132}Sn beam at 4.33, 17.0 and 22.4 MeV/u, respectively. Charge state distributions for ^{132}Sn at these three possible energies are given in tables 4 and 5. Pardo's formula [30] has been proven to fit the experimental data at a few MeV/u in years of experiments in ATLAS. As mentioned by Leon *et al.*, the Ganil formula [31] fits best the data for energy above 18 MeV/u. Nevertheless, the Ganil formula fits stripping of Nickel also at lower energies as 10-12 MeV/u [32] and hence we used it for stripping at 17 MeV/u too.

Table 4: Charge state distribution in % for ^{132}Sn @ 4.28 MeV/u passing through a carbon foil. Values are calculated assuming steady state and using three different references. The distribution curves are in figure 5.

Charge state (q)	P(q) (%) Ganil [31]	P(q) (%) Sayer [33]	P(q) (%) Pardo [30]
32	1.85	0.40	0.48
33	5.22	1.38	1.63
34	11.10	3.89	4.33
35	17.73	8.78	9.02
36	21.28	15.55	14.76
37	19.18	21.10	18.95
38	12.99	21.38	19.11
39	6.61	15.72	15.13
40	2.53	8.11	9.41
41	0.73	2.83	4.59
42	0.16	0.64	1.76
Average q	36.14	37.55	37.53
Sum of 5 q (%)	82.3	82.5	77.4

Table 5: Charge state distribution in % for ^{132}Sn @ 16.6 and 22.0 MeV/u passing through a carbon foil, calculated assuming steady charge state and using the Ganil formula [31].

Charge state (q)	P(q) (%) 16.6 MeV/u	P(q) (%) 22.0 MeV/u
43	1.13	
44	6.81	0.14
45	20.84	2.32
46	32.49	14.73
47	25.80	35.84
48	10.43	33.37
49	2.15	11.89
50	0.23	1.62
Missing fraction (%)	0.0	0.1
Average q	46.15	47.43
Sum of multi-charge (%)	96.0	95.8

In the 2-strippers mode of operation, the distribution after the first stripper is calculated by means of the Pardo's formula [30]. The five more populated charge states

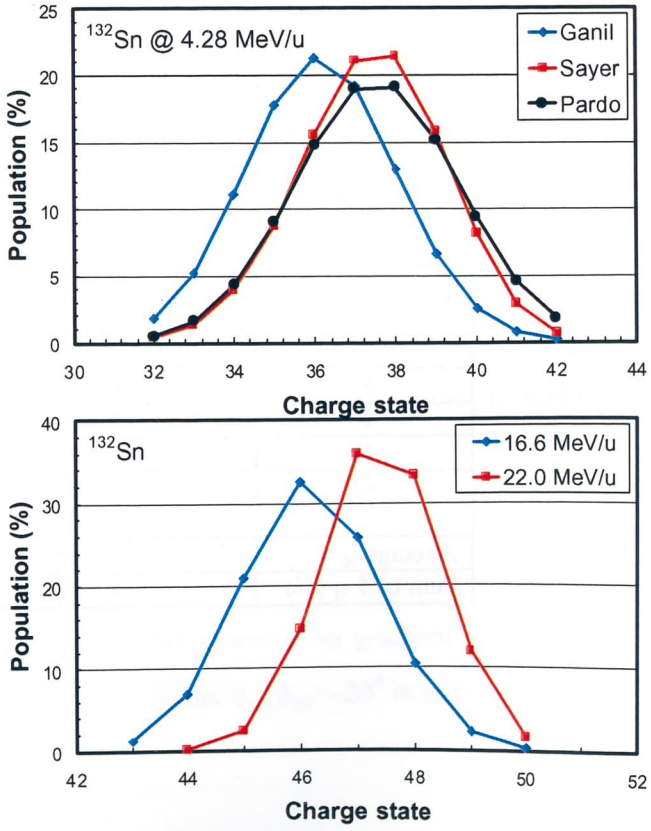

Figure 5:
Tope: Equilibrium charge state distribution for ^{132}Sn at 4.28 MeV/u passing through a carbon foil, calculated using the three formulas mentioned in the text. (Same information as in table 4).

Bottom: Equilibrium charge state distribution for ^{132}Sn passing through a carbon foil at the position of the second stripper. Calculated using the Ganil formula. (same information as in table 5).

include 77 % of the beam particles. For the second stripper the Ganil formula [31] is used and 4 charge states are transported with 96 % efficiency. The total transmission after the two strippers, in this case, is 74 %. In the one-stripper mode of operation, five charge states are transported with 96 % efficiency (table 5). The efficiency of 100 % can be reached only in the case of acceleration without stripping.

4.3 Energy evolution

The energy evolution and TTF for the proposed scheme of the post-accelerator are shown, for the reference beam in the three modes of operation, in figures 6-8, and for two other possible radioactive beams in figures 9 and 10. The TTF, calculated using eq.(2), is normalized to unity at the optimum β_0 given in table 2. The energy is calculated using eq.(3); the resonators accelerating gradient is 7 MV/m. The input and output energy and the transmission of each section are given in table 6.

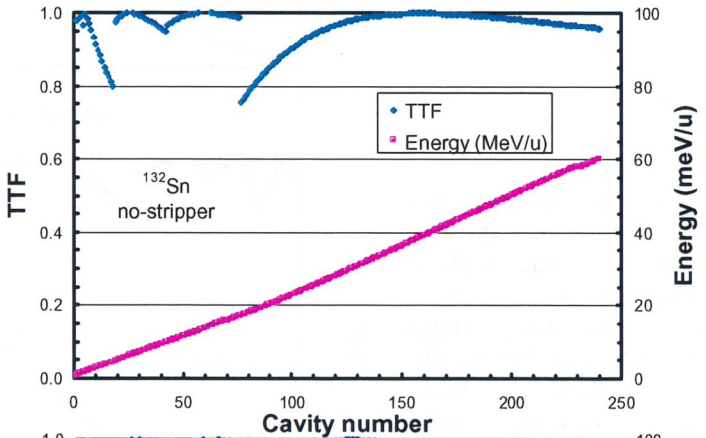

Figure 6: The $^{132}Sn^{25+}$ beam energy and TTF (normalized) profiles with no stripper, for best beam quality and full intensity up to 60 MeV/u.

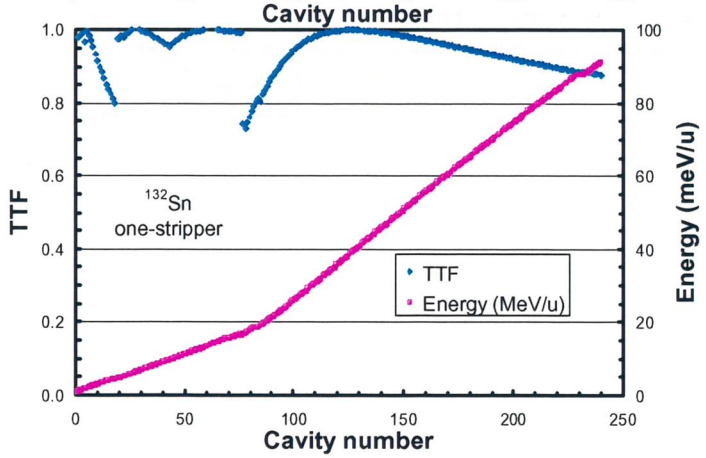

Figure 7: The ^{132}Sn beam energy and TTF (normalized) profiles in the 1-stripper mode of operation, with only the second stripper. The reference charge after the stripper is 45+ and 5 charges are transported simultaneously up to 91 MeV/u.

Figure 8: The ^{132}Sn Beam energy and TTF (normalized) profiles along the linac with 2 strippers, for maximum final energy.

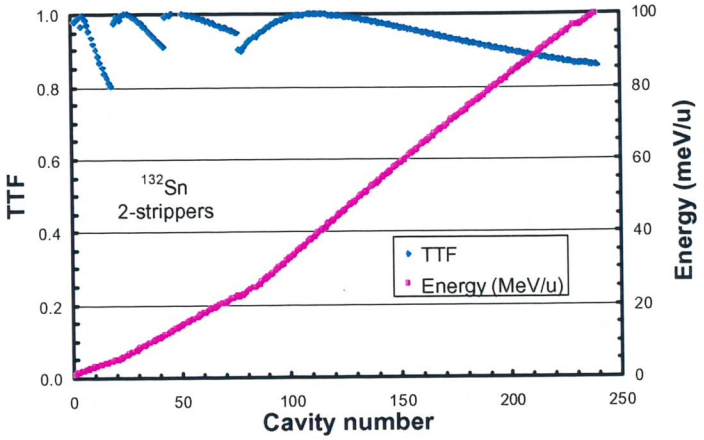

Figure 9: Energy and TTF (normalized) profiles along the linac with 1-stripper for a light beam of ^{33}Ar at charge states 8+, and 17+ at the low, medium and high-energy sections. Final maximum ion energy is 130 MeV/u.

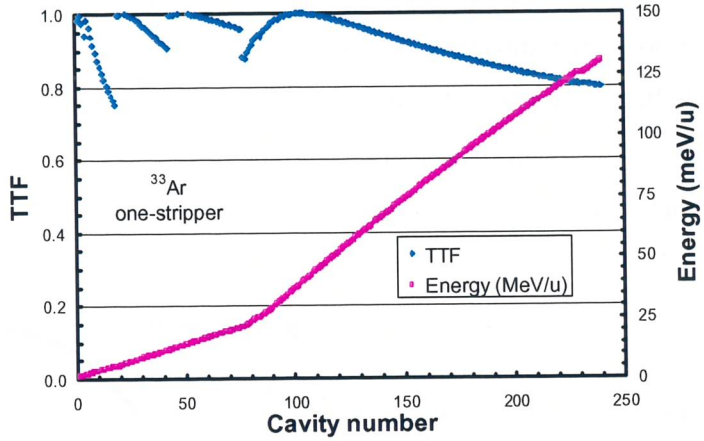

Figure 10: Energy and TTF (normalized) profiles along the linac with 2 strippers for a heavy beam of ^{210}Fr at charge states 25+, 52+ and 73+ at the low, medium and high-energy sections. Final maximum ion energy is 96 MeV/u.

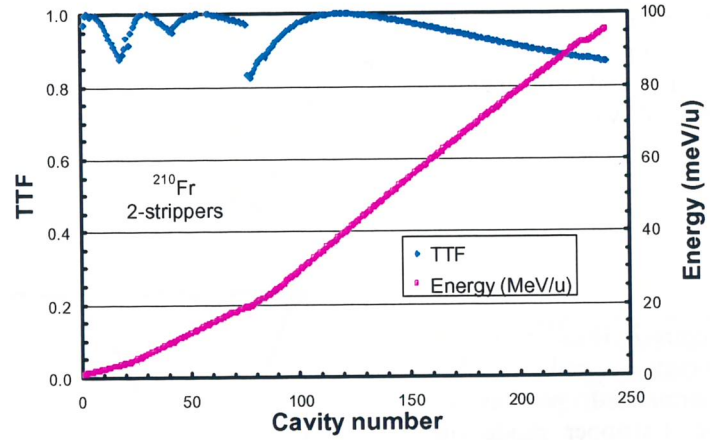

Table 6: Linac configuration and beam parameters, of the $^{132}Sn^{25+}$ case and other radioactive beams, for the three possible operation modes. The energies are calculated using eq.(3) and acceleration gradient of 7 MV/m. The stripping probabilities are calculated as explained in section 4.2. The reference charge states are bolded. (I/O=input and output of section).

Energy Section		**Low**		**Medium**		**High**	
Number of cryostats		2		15		20	
Total length (m)		7.5		30		76	
Resonator	Type	QWR		QWR		HWR	
	Number	4	14	24	34	164	
	Optimum β (%)	4.7	5.5	11	16.5	28	
	Frequency (MHz)	80	80	160	240	320	
Solenoid	No. of cavities per solenoid	4 (5)		4		8	
	Length (cm)	30		30		45	
	Max. field (T)	15		15		15	
^{132}Sn Two strippers mode	Transported charge states	25		36,**37**,38,39,40		46,**47**,48,49	
	I/O Energy (MeV/u)	0.67	4.4	4.2	22.5	21.6	100.2
	Ion transmission (%)	100		77		96	
	Overall Ion transmission (%)	74					
^{132}Sn One Stripper mode	Transported charge states	25		25		44,**45**,46,47,48	
	I/O Energy (MeV/u)	0.67	4.4	4.4	16.8	15.1	91.1
	Ion transmission (%)	100		100		96	
	Overall Ion transmission (%)	96					
^{132}Sn No stripper mode	Charge states	25		25		25	
	I/O Energy (MeV/u)	0.67	4.4	4.4	17.0	17.0	60.2
	Ion transmission (%)	100		100		100	
	Overall Ion transmission (%)	100					
^{132}Sn Two strippers mode Low breeding case	Charge states	13		31,**32**,33,34,35		45,**46**,47,48	
	I/O Energy (MeV/u)	------	2.7	2.6	18.4	16.7	94.6
	Ion transmission (%)	100		78		92	
	Overall Ion transmission (%)	72					
^{33}Ar One Stripper mode	Charge states	8		8		16,**17**,18	
	I/O Energy (MeV/u)	0.67	5.3	5.3	21.2	19.2	129.9
	Ion transmission (%)	100		100		~100	
	Overall Ion transmission (%)	~100					
^{210}Fr Two strippers mode	Charge states	27		51,**52**,53,54,55,56		72,**73**,74,75,76	
	I/O Energy (MeV/u)	0.67	3.3	3.2	19.4	17.6	95.5
	Ion transmission (%)	100		76		77	
	Overall Ion transmission (%)	59					

4.4 Design in the absence of very high charge breeding

Research and development in the field of charge breeders is presently very active, and promising results have been obtained [34]. However, the performance of present systems decrease significantly for high charge state, and beams like the nominal ^{132}Sn cannot yet be produced in the 25+ with good efficiency. We analysed the SRL linac performance

with low-charge ^{132}Sn beams that can be delivered either by existing charge breeders, or that can reasonably be expected to be available in a few years from now. In all following cases the beam transport option without stripping has been excluded, since it would not allow reaching the required 100 MeV/u with acceptable linac cost.

- Breeder case of q=13+

The linac would in this case require only 12 more low-beta cavities to boost the beam up to the first stripper. The proposed 3-RFQ injector is already suitable for this application. The increase in LINAC length would be minimum (~5 m) as well as the increase in the total cost (~4%).

- Breeder case of q=6+

For A/q = 22, the SC RFQ section should be doubled (e.g. 6 RFQs instead of 3) and 21 more cavities than in the nominal case would be required to reach 100 MeV/u. The cost, compared to the 25+ case, would increase by about 12%.

- Without breeder, case of q=1+

For this case, the linac design above 0.67 MeV/u would not change significantly from the nominal case; however, a major effort would be required to accelerate a q/A= 1/132 beam up to this energy. This problem was studied by Ostroumov *et al.* for the RIA post-accelerator; a solution was proposed based on 2 RFQs mounted on a 380 kV platform, followed by a third RFQ at ground potential and by about a 50 m long superconducting linac [35]. The cost of this system is comparable with the cost of the rest of the post-accelerator. This solution, although feasible, is very expensive.

Since the linac design from about 0.67 to 100 MeV/u does not depend significantly on the initial beam charge state, this part of the linac can be the same, no matter whether a charge breeder is available or not. The linac solution for the EURISOL post-accelerator is therefore less sensitive to the charge breeder performances relative to other solutions based on cyclotron technology.

5 Real field distribution

Beam dynamics in the different sections of the nominal linac have been simulated by means of the LANA 3D code [13,14]. LANA allows input files containing realistic, non-symmetric, electromagnetic field distributions in accelerating cavities, which can be

calculated with good precision by means of many available codes. The field distribution of the cavities used in this work have been calculated by V. Zviagintsev by means of the code HFSS (High Frequency Structure Simulator) [36]. Examples of real field components are shown in figure 11. The fields are normalized before introducing them in LANA so that the total acceleration energy gain will be as calculated by the analytical formula (section 4).

The real field for all cavity types was calculated in a grid with a finite number of points. LANA transforms the HFSS Cartesian coordinates into cylindrical coordinates and

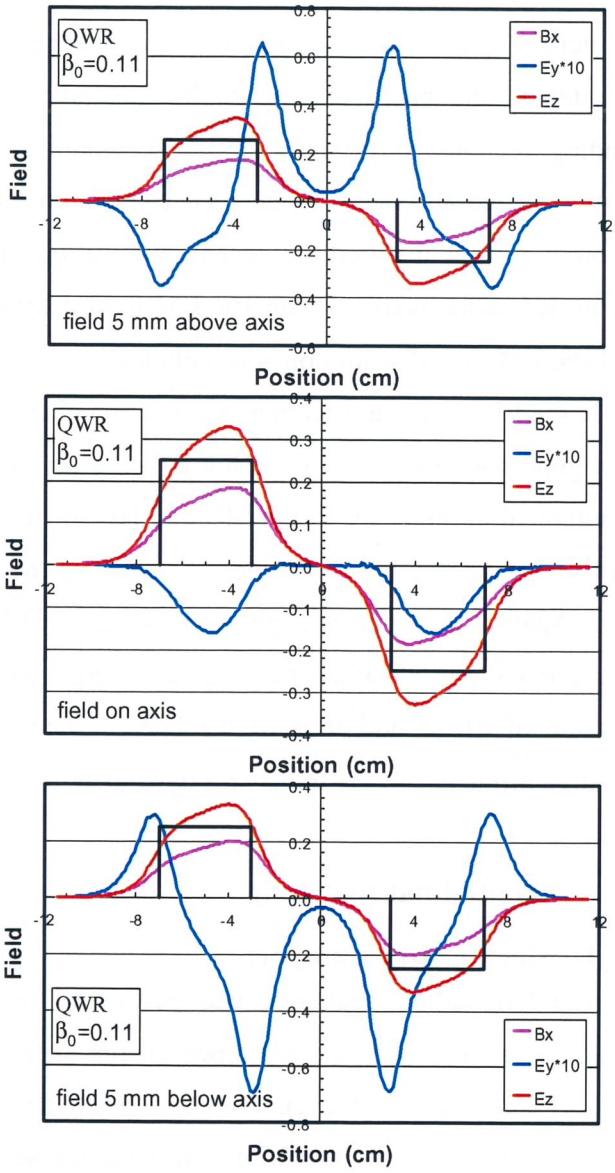

Figure 11: Real field distribution in a QWR optimized for β_0=0.11, on axis (middle), above (top) and below (bottom) axis. The fields are shown in a right hand cartesian coordinates with origin in the middle of the drift tube, where Z is the beam direction and Y is pointing up. The three field components are given in arbitrary units. For clarity, the transverse electric component Ey is shown with a factor 10 magnification, and Bx is shown with 90^0 phase delay. The black squares represent the location of the acceleration gaps.
The field was calculated with HFSS using a 1 mm pitch grid in the resonator drift tube region.

calculates the field between points of the grid by means of field interpolation. We verified that this grid resolution is sufficient to describe the effects of asymmetric fields typical of quarter- and half-wave resonators.

6 Beam dynamics simulation

The simulations have been performed, using LANA [13,14], for each energy section separately. The initial transversal distribution in all sections is a 4D ellipsoidal uniform distribution; in the longitudinal phase space, the particles are randomly distributed inside the defined phase space ellipse of a given emittance. The stripper effects have been included to the beam divergence by quadratic sum. We assumed that multi-charge bending sections, if properly designed, would have a minimum effect on the beam quality. In the absence of a detailed calculation their contribution was not taken in to account; this is justified by recent publications [27]. The first simulation has been performed using axially symmetric EM field distribution in accelerating gaps. Later, the realistic EM field distribution was included.

In the LE section a reference acceleration phase of -20^0 was chosen. This appeared to be a good compromise to have low QWR steering [9], high acceleration and sufficient longitudinal acceptance. In the ME and HE sections, where multiple charge transport is performed, we chose as reference charge state the most populated one lowered by one unit. Again, the reference phase was -20^0. Different charge states have different synchronous phase values for a given energy gain. In QWR, however, steering is a function of phase and thus of the charge state (see section 6.2.1). This can have a negative influence on the transverse dynamics.

6.1 Longitudinal matching

6.1.1 Single charge transport

The longitudinal matching was performed first by optimising the beam transport along the all linac for the reference charge state, at the nominal accelerating field (7 MV/m) and phase (-20 deg). The input beam parameters were set in order to keep the bunch length (in ns) along the three acceleration sections as a slowly decreasing function.

To keep the bunch length within acceptable limits, a compact design was necessary for the low energy section, with one diagnostic box located between the two long cryostats (fig.3, top) hosting eight cavies and two solenoids each. The medium- and high-energy sections cryostats include, together with one solenoid, four or six cavities, respectively, and are followed by a diagnostic box.

6.1.2 Energy loss and emittance growth in strippers

The beam straggling and energy loss in the SRL strippers are not negligible, and had to be included in the calculations. In order to minimize emittance growth, the stripper foils have been located in a longitudinal and transverse beam waist. This could be done easily in the LE section, without modifying the acceleration lattice. In the ME one, a special bunching section was required in order to re-bunch the multi-charge beam.

In order to allow the SRL beam particles to reach a steady state charge distribution in the strippers (the so-called equilibrium), and in order obtain the highest charge state and a narrower distribution, rather thick foils are needed [31]. The stripper thickness requirements for high charge state and good beam quality, however, are somehow contradictory [23]: the thicker is the foil, the more beam scattering, beam losses and emittance growth are produced. The values that we have used are shown in table 7. The longitudinal and transversal straggling have been calculated with a semi-empirical analytical formula using the code IRMA [37], and with simulation based on semi-empirical formula using the code SRIM [38]; in both cases, carbon foil strippers were assumed. IRMA was developed based on low energy heavy ions experimental data, and SRIM [39] on light ions up to energy of 10 GeV/u. There is a discrepancy of about one order of magnitude between the energy straggling values calculated with the two formulas, as shown in table 7. The few available experimental data on heavy ion stripping in carbon foils (see [40,41,42,43]) at the EURISOL energy, seem to show a much larger energy straggling than predicted by SRIM. [23]. To keep a conservative approach, when the choice between the IRMA and the SRIM results was not supported by experimental data, we decided to use the most pessimistic ones.

Table 7: Stripper effects for the two modes of operation in multi-charge beam transport.

Stripper station		1	2	2
Mode of operation		2 strippers	2 strippers	1 stripper
Stripper thickness ($\mu g/cm^2$)		200	3000	2000
Incident energy (MeV/u)		4.347	22.435	16.988
Energy loss (keV/u)	IRMA	98	843	647
	SRIM	107	922	708
Energy loss (%)		2.4	3.9	4.0
Incident rms energy straggling (keV/u)		4.74	13.0	9.85
Energy rms straggling (keV/u)	IRMA	1.30	4.1	3.59
	SRIM	0.18	0.47	0.36
Longitudinal emittance growth (%)		3.7	4.9	6.5
Incident rms straggling (mrad)		2.0	1.0	0.7
Transversal rms straggling (mrad)	IRMA	0.57	0.60	0.63
	SRIM	1.1	0.75	0.80
Transversal emittance growth (%)		14	30	52

6.1.3 Multi-charge beam transport

The rather large acceptance of superconducting linacs allows simultaneous acceleration of different charge states. The best beam quality can be achieved if the synchronous phase, for each charge state, is set according to the following formula [7]:

$$\phi_q = -\arccos(q_0/q \cos(\phi_0)) \qquad (4)$$

where q_0 and ϕ_0 are the reference charge and its synchronous phase. In this configuration, different charge states are accelerated in different bunches of small emittance, travelling at the same speed. The non-linear configuration described by formula [7] can be approximately obtained by means of a simple rebunching/debunching system at each stripper. The aim is to collect all charge states in a single bunch in the stripper for minimum emittance growth, and to align all new charge states after the stripper according to formula [7], or to a linear approximation of it, which is anyhow satisfactory and more easily achievable.

The values used in the first simulation are shown in table 8.

Table 8: Synchronous phase calculated using equation (4) (2nd column); the phase-shift relative to the reference charge (3rd column); the linear approximation of eq. (4) (4th column) and the result of phase synchronization used in the final beam dynamics (5th column).

Charge state	Optimum Synchronous phase (deg)	Optimum Phase shift (deg)	Linear approximation of the optimum phase shift (deg)	Result of phase synchronization (deg)
ME section				
36	-15.0	5.0	3.2	2.3
37	-20.0	0	0	-0.2
38	-23.8	-3.8	-3.2	-2.8
39	-26.9	-6.9	-6.4	-5.4
40	-29.6	-9.6	-9.6	-7.8
HE section				
46	-16.2	3.8	3	
47	-20.0	0	0	
48	-23.1	-3.1	-3	
49	-25.7	-5.7	-6	

6.1.3.1 Phase synchronization of the multi-charge beam

The main effect of a thin stripper foil to the bunched beam, in addition to changing its charge distribution and giving some energy loss, is a sudden increase of the transversal and longitudinal spreads $\Delta x'$, $\Delta y'$ and ΔE; this gives an emittance increase proportional to the beam size Δx, Δy and Δt at the stripper. For this reason, in order to limit emittance growth, the beam can be strongly focused on the stripper, both longitudinally and transversally. The foreseen beam current is low enough to guarantee that the power density in the stripper is not sufficient to damage it.

The multi-charge beam transport simulation starts, after each stripper, with all bunches of different charge state ("q-bunches" from now on) superimposed in the same phase space. The first few cavities must be used to bring each q-bunch close to its ideal synchronous phase (see table 8). This can be obtained rather naturally, since q-bunches with higher charge are pushed toward higher (i.e. more negative) phase values during acceleration.

In the ME section, the multi-charge separation is done by operating the first two cavities at phase $\phi_0=-15^0$. The third one, located after a drift in a solenoid, is operated at

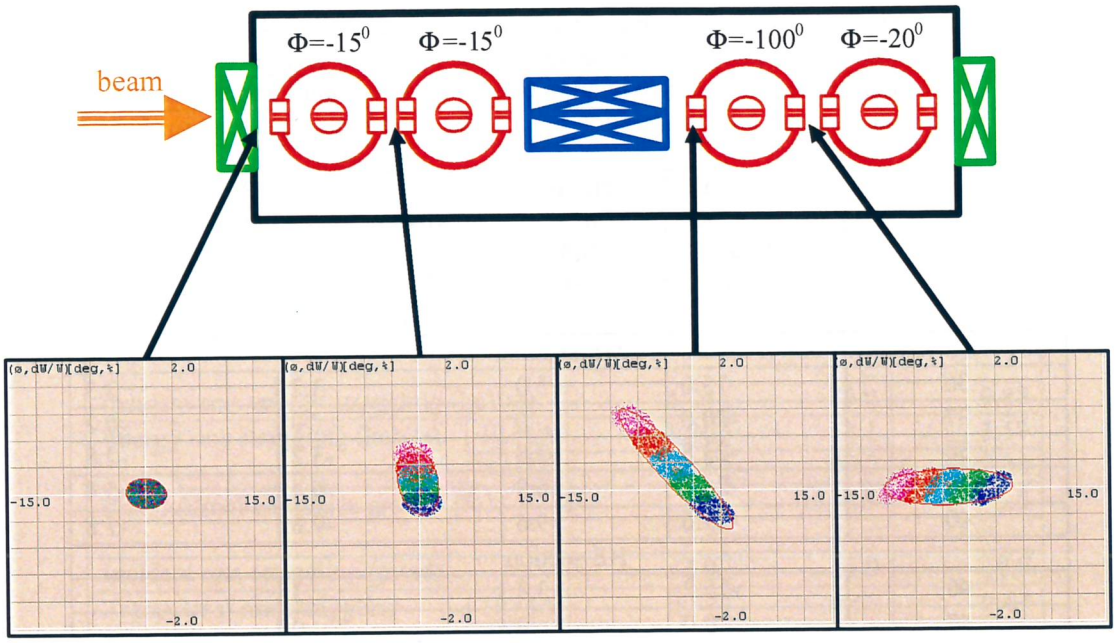

Figure 12: Phase synchronization after the first stripper, at the beginning of the ME section. Top: first cryostat (see fig 3) and the reference acceleration phase at each of the cavities. Bottom: longitudinal phase space, in energy spread (%) as function of phase (deg) in different position along the cryostat. The cavities frequency is 160 MHz. The 5 charge states of the beam particles are represented by different colors.

$\phi_0 = -100^0$ as a rebuncher (see figure 12), bringing again all charges to the same velocity. At the entrance of the forth cavity, all five selected q-bunches are located close to their ideal synchronous phase, where they stay during acceleration until the cavity frequency is changed or a stripper is met.

In the HE section, after the second stripper, the first eight cavities are needed to reach phase synchronisation at the entrance to the second cryostat. The required rf phases are $\phi_0 = -10, -10, -10, -10, -10, -35, -45, -100^0$.

In both ME and HE section, only one cavity is used just for bunching without giving significant acceleration.

6.1.3.2 Multi-charge re-collection section before stripping

Bunching on the first stripper can be done by means of the regular linac lattice of the LE section. The second stripper, at the end of the ME section, requires a longer bunching-re-collecting system; the bunching section is illustrated in figure 13. The last cavity of the

regular lattice is operated at a bunching phase of -90^0, and followed by a 1.1 m long drift. This gives a charge-dependent energy gain which move all charge states toward the same -20^0 phase; the next six QWRs, housed in a special cryostat, give both acceleration and debunching to obtain a unique bunch at the stripper.

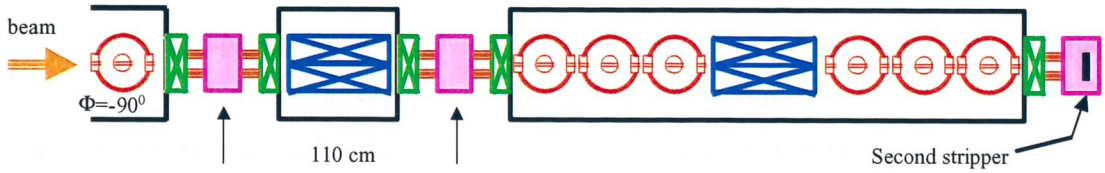

Figure 13: Bunching section at the end of the ME line, before the second stripper. See fig.3 for the symbols definition. The last cavity of the regular linac lattice (on the left) is operated at a bunching mode. At the entrance to the last cryostat the beam is nearly bunched. The last six cavities are acting as de-bunchers in order to bring all charges to the same energy.

To bunch the multi-charge beam at the HE experimental area, a similar but longer bunching section is needed. The last three cavities of the regular HE section lattice are set at -90^0 rf phase; the beam then goes through a 7 m drift which includes two, 45 cm long solenoids. The last cryostat is a regular HE section type cryostat with eight HWRs, used as multi-charge re-collector; the rf phases of the cavities are between -10^0 and -20^0. The bunching section length was optimised for the reference beam; however, by only modifying gradient and phase settings, it can be used with all other beams foreseen in EURISOL.

6.2 Transversal matching

The main parameter that we have used for the transversal matching is the phase advance per period. The initial value was 90^0, that is in the middle of the stable phase advance interval [29]. However, QWRs produce vertical steering and, consequently, different phase advance in the two transversal phase spaces. This is particularly evident in a focusing system based on solenoids, where the focusing strength on the two planes is, by construction, the same.

Concerning the emittance growth induced by the strippers, we used in the calculation the transversal straggling given by the code SRIM.

6.2.1 Tuning based on phase advance per period

The phase advance per period is determined by the solenoid gradient, the defocusing power of the cavities, the number of cavities per period, the electric and magnetic rigidity of the beam particles. Ostroumov [15] proposed for the RIA driver linac a phase advance per period of 60^0. Comparing to the RIA case, we have more cavities per solenoid and higher accelerating field. In this configuration an average phase advance in the range of 90^0-115^0 was found to minimize the beam envelope size and emittance growth. The phase advance per period φ in the transverse phase space is defined as (see for example [29] page 207):

$$\varphi=\int ds/\beta \qquad (5)$$

where *ds* is the interval along the beam direction (in cm in the present paper) and β is the Twiss parameter (in cm/rad).

In our configuration, with one solenoid in the center of the cryostat (fig. 3), we define a period starting at the center of a solenoid and ending at the center of the next one. A period of the medium energy sections, for the β_0=0.11 and 0.165 QWR, is described in table 9 (see fig.3).

Table 9: Period breakdown in the ME section.

Description of interval	Length (cm)
half a solenoid	15
drift	5
cavity	23
cavity	23
drift	32
diagnostics	
drift	32
cavity	23
cavity	23
drift	5
half a solenoid	15
Total	196

The phase advance per period φ is calculated numerically, by means of eq.(5), using the Twiss parameter β given by the LANA code. It is calculated separately for x and y (and z) directions. The initial Twiss β value is set close to twice the period length divided by the chosen phase advance (see page 7 of [15]).

The solenoids were tuned by keeping constant $(\varphi_x+\varphi_y)/2$, the average phase advance per period in the x and y planes. The calculated value is sensitive to the number of particles in the simulation. The random error in a simulation with only 500 particles is about $\Delta\varphi=\pm 5$ %. This is considerably reduced by using 5000 particles or more in the simulation, but this doesn't result in significant change of the beam quality at the end of the section.

The linac tuned with this technique for the reference charge state allows also multi-charge beam transport. Table 10 compares the beam quality for different choices of phase advance and reference charges in the ME section. This table shows that, in order to minimize the final total emittance, the phase advance must be adjusted, period by period, between 110^0 and 115^0. It should be noticed that no difference was found, in the ME section made of QWRs, between constant and alternate solenoid field polarity (on the contrary, a clear effect was found in the HE section made of HWR, see discussion in section 6.2.3).

Table 10: Comparison between different methods of transversal tuning of the medium energy section, after the first stripper. The multi-charged beam is ^{132}Sn in the 5 charge states 36,37,38,39,40. The solenoids polarity is either constant or alternate. (Note: the initial beam parameters of this table are not the nominal ones used later).

Case number		1	2	3	4	5
Simulation parameters:						
Reference charge state	transversal	37	38	37	37	37
	longitudinal	37	37	37	37	37
Average phase advance (deg)		90	90	90	110	110-115
Solenoid field polarity		Alternate	Alternate	Constant	Alternate	Alternate
Number of particle in simulation		2500	2500	4000	4000	4000
Simulation results at the exit of ME section:						
Maximum beam size inside cavities at the ME section (cm)		0.6	0.6	0.7	0.6	0.6
Transversal rms emittance (π cm mrad)	X	0.015	0.016	0.016	0.015	0.014
	Y	0.019	0.020	0.017	0.017	0.012
Longitudinal rms emittance (π keV/u ns)		0.83	0.84	0.89	0.86	0.89
Volume (mm^2 $mrad^2$ keV/u ns)		0.73	0.83	0.75	0.68	0.46

An example of transversal phase advance values along the high-energy section of the EURISOL post-accelerator is shown in figure 14.

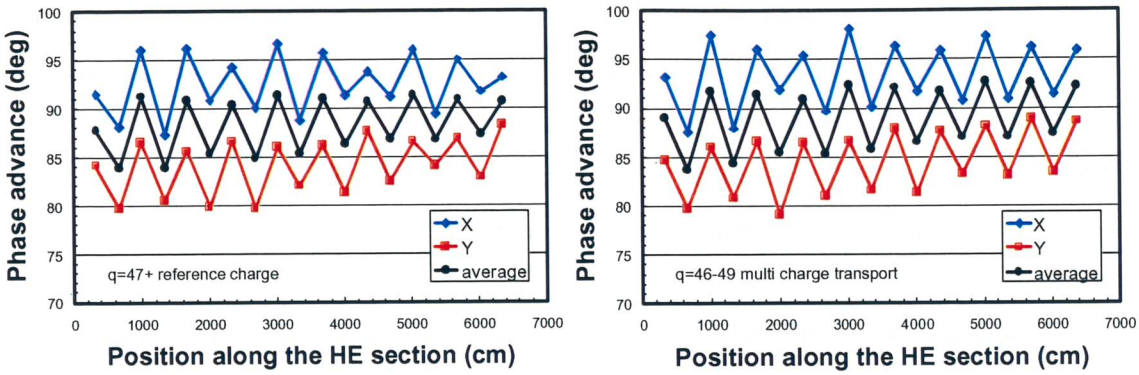

Figure 14: Phase advance per period along the high-energy section. Left: reference charge state (simulation with 800 particles). Right: all charges with the same linac tuning as before (simulation with 4000 particles).

6.2.2 Solenoids field

The solenoid length is determined by the requirements of 10 T maximum field. This is 2/3 of the maximum rated today for commercial SC solenoids with bore radius of up to 2.5 cm [44]. This is much larger than the cavity bore radius (1 cm) used in the beam transport simulation. To account for the mechanical length of the solenoids, a drift space of 10 cm was added to their effective length. This lattice design is rather compact, but feasible with the today technology. Laxdal and Pasini [20] assumed for the design of ISAC-II that any solenoid with a bore diameter of 3 cm requires 7.8 cm on either sides of the effective field boundary to define the mechanical length.

In this work we used 30 cm long solenoids (effective length) in the LE and ME sections, and 45 cm long ones in the HE section. The solenoids field, for the ^{132}Sn beam and 2-stripper mode, could be kept below 10 T for all solenoid but one (figure 15). The last solenoid in the standard lattice of the ME section (before the bunching section in front of the second stripper) required a higher field. Two HE solenoids were then introduced in the bunching section at the end of the ME section.

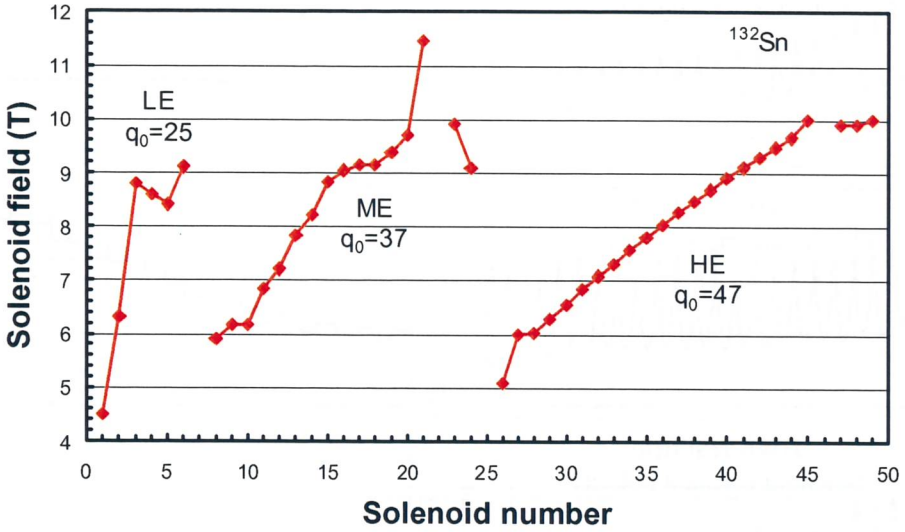

Figure 15: Solenoid field along the EURISOL post-accelerator for the ^{132}Sn beam and 2-stripper mode of operation. Note that the horizontal axis is the solenoid index and not a real estate position. The separated solenoids at the end of the ME and HE sections belong to the bunching section.

6.2.3 Quadrupole effect

In the HE section the rf frequency is 320 MHz. This allows using conveniently HWRs in place of QWRs. HWRs, although free from the steering effect present in QWRs, possess a quadrupole field component. In the HWR geometry used for the simulation, with a cylindrical internal conductor as in the LNL type QWR, the quadrupole effect may introduce a visible effect: for the case of alternate solenoid polarity, emittance growth as high as 50 % along the HE section was observed (see figure 16). In the case of constant polarity orientation, however, the x and y phase spaces mixing produced by solenoids causes emittance exchange in the two planes but no increase of the average emittance even in the presence of quadrupolar field (fig.16.c).

Resonator shaping, (e.g. as suggested by Pasini and Laxdal [19]) can reduce the quadrupole effect to some extent.

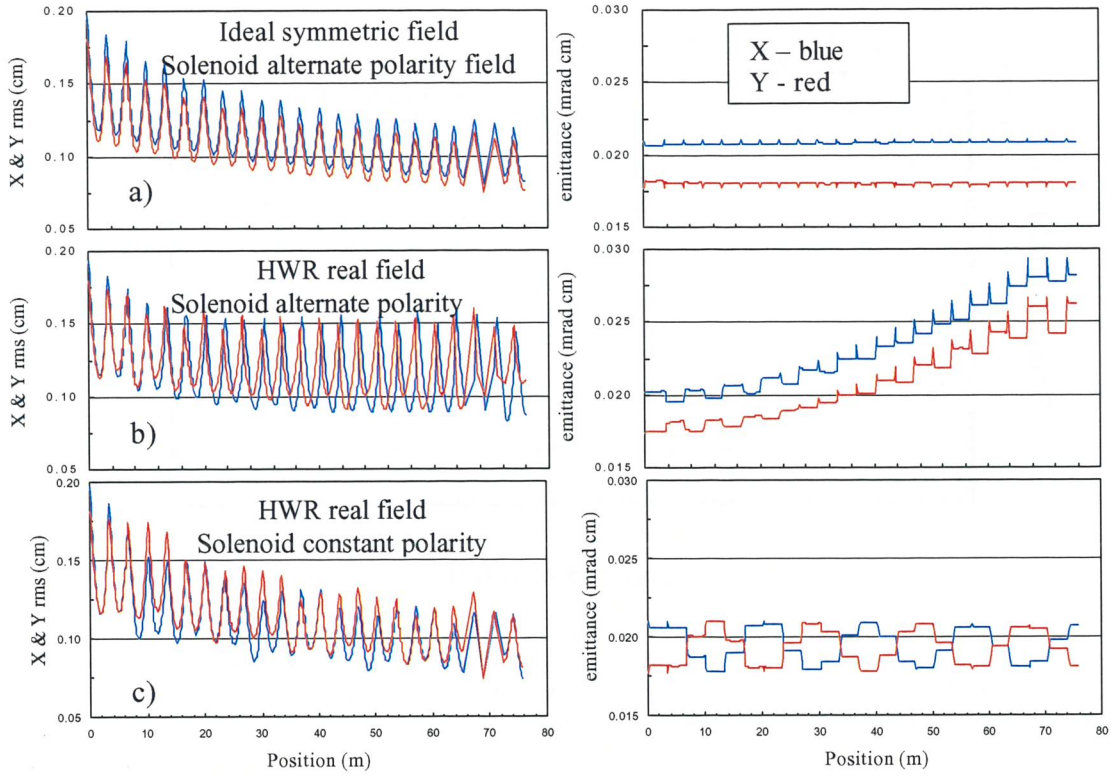

Figure 16: Beam envelopes (left) and transversal rms emittance (right) along the HE section. a) ideal symmetric EM field in the resonators and alternate orientation of the solenoids field; b) realistic EM field in the HWR and solenoids field with alternate orientation; c) realistic EM field in the HWR and constant orientation solenoids field.

6.2.4 Longitudinal phase advance

Space charge produces coupling of the longitudinal and the transversal phase spaces [45]. In high intensity beam linacs, crossing of the transverse and longitudinal phase advance values may cause mismatch, emittance exchange and emittance growth. Although the EURISOL post-accelerator is dealing with low intensity beams, we checked possible correlation between phase advance crossing and emittance growth. In Ref. [45] longitudinal phase advance smaller than the transverse, *i.e.* around 75^0, is recommended to avoid crossing.

In this work, the longitudinal phase advance is calculated using the LANA longitudinal Twiss parameter β_z. The following transformation is used to express longitudinal and transversal phase advance in the same units:

$$z = \phi * \beta\lambda/2\pi \quad \text{or}$$

$$z(\text{cm}) = 83.276 * \beta * \phi(\text{deg}) / f(\text{MHz}) \quad \text{longitudinal unit} \quad (6)$$

$$z' = (\Delta E/E) / (\gamma * (\gamma+1)) \quad \text{or}$$

$$z'(\text{mrad}) = 10 * \Delta E(\%) / (\gamma * (\gamma+1)) \quad \text{long. divergence unit} \quad (7)$$

$$\beta_z(\text{cm/mrad}) = 8.3276 * \beta * \beta_z(\text{deg}/\%) * (\gamma * (\gamma+1) / f(\text{MHz})) \quad (8)$$

where E is the kinetic energy, β (without subscript) and γ are the relativistic particle parameters and z is the particle longitudinal coordinate relative to the reference particle. The particle velocity β is assumed to be approximately constant in the cavity.

In the linac design the periodicity of β_z, differently from the ones of β_x and β_y, is not linked to the lattice periodicity, but varies during acceleration. The envelope shape is mainly determined, in addition to the initial parameters, by the gradient and synchronous phase chosen to optimise multi-charge beam transport. Based on the assumption that at the low-intensity beam the phase advance crossing does not cause problems, in the present work the longitudinal phase advance was not kept constant, and was not used as a tuning tool. An example of a longitudinal phase advance at the HE section is shown in figure 17. Indeed, no correlation was found between phase advance crossing and emittance change in this linac.

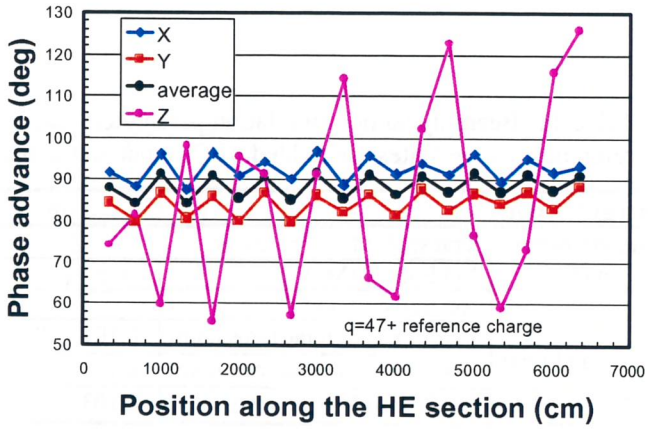

Figure 17: longitudinal and transversal phase advance per period in the HE section of the EURISOL post accelerator.

6.3 Emittance

The simulation parameters and the results of the EURISOL post-accelerator are summarized in table 11 for the 2-stripper mode. The emittance is given in table 11 and in figure 18, and the beam envelopes in figure 19. In the 2-stripper mode, significant emittance growth can be observed in the ME section. The causes are QWR steering, multi-charge beam transport with imperfect phase synchronization (e.g. after the change of frequency in the middle of the section), imperfect bunching and charge recollection at the end of the section. The bunch shapes in the longitudinal phase space are shown in figure 20. No significant tail is developed along the accelerator. In the HE section there is no transversal emittance growth, but a strong exchange of emittance between the two transversal phase spaces, as explained in section 6.2.3. The QWR steering effect can be seen, in the LE and especially in the ME sections, by comparing the x and y envelopes of fig. 19: the beam size appears to be larger, and oscillating, in the y direction due to the displacement of the beam off axis. In the HE section, where HWRs are used, this effect disappeared. It is interesting to note that, although the linac is tuned on the reference charge, the transversal beam size does not increase significantly when all charges are transported.

The beam size is maximum at the solenoid centre positions, where the bore radius is 20 mm. Inside cavities, the beam size never exceeds 5 mm, i.e. half of the bore radius (except for the first two QWRs of the ME section, where the maximum beam radius is 6 mm).

Table 11: Beam dynamics simulation parameters and results of the $^{132}Sn^{25+}$ case. The reference charge states are bolded. (I/O=input and output of the section).

Energy Section		**Low**		**Medium**		**High**	
Two strippers mode	Transported charge states	25		36,**37**,38,39,40		46,**47**,48,49	
	I/O Energy (MeV/u)	0.67	4.3	4.2	22.4	21.6	100
	Ion transmission (%)	100		77		96	
Initial and final emittance	I/O X (π mm mrad) rms norm.	0.101	0.107	0.123	0.159	0.210	0.208
	I/O Y (π mm mrad) rms norm.	0.102	0.107	0.123	0.136	0.177	0.182
	I/O Z (π keV/u ns) rms	0.103	0.109	0.113	0.263	0.276	0.335

For the other modes of operation (no-stripper and 1-stripper mode with multicharge beam) the simulations have been performed giving the correct synchronous phase values as initial parameters (see section 6.1.3), i.e. no further simulation was done of the bunching sections.

Compared to the "2-stripper" mode values, the final transversal and longitudinal emittances of the "1-stripper" mode are 65% and 70%, respectively, and 55 % and 35 % in the "no stripper" mode.

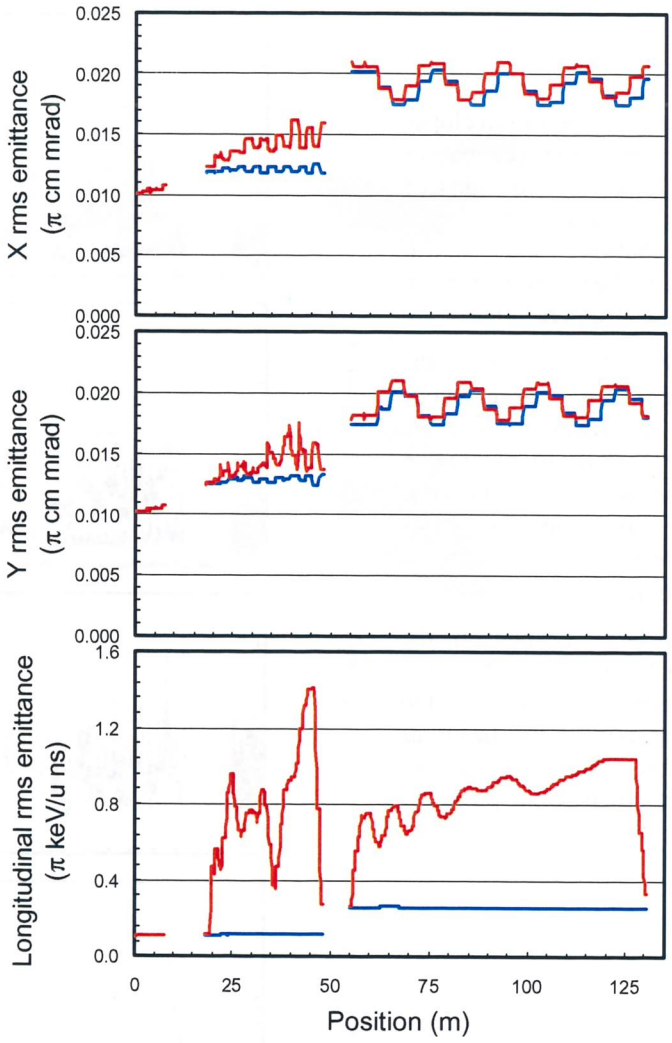

Figure 18: Normalized rms emittances along the EURISOL post-accelerator, simulated for the test beam ^{132}Sn in the "2-strippers" mode of operation. The beam parameters given in table 11. The lower blue curve is the emittance of the reference particle beam; the upper red curve is the emittance of the multi-charge beam. The origin of the sharp changes in the emittances is not physical but related to the numerical calculation done by the code LANA. The strippers' positions are represented by gaps in the plots. The large change in the longitudinal emittance after the strippers reflects the multi-charge phase synchronization.

The rms emittance of the beam is calculated from the particle distributions by means of the usual formulas:

$$\bar{x} = \frac{1}{N}\sum x_i, \quad \overline{x^2} = \frac{1}{N}\sum x_i^2, \quad \bar{x'} = \frac{1}{N}\sum x_i', \quad \overline{x'^2} = \frac{1}{N}\sum x_i'^2,$$

$$\overline{xx'} = \frac{1}{N}\sum x_i \cdot x_i',$$

$$D_x = \overline{x^2} - \bar{x}^2, \quad D_{x'} = \overline{x'^2} - \bar{x'}^2, \quad D_{xx'} = \overline{xx'} - \bar{x} \cdot \bar{x'},$$

$$\varepsilon_x = \sqrt{D_x \cdot D_{x'} - D_{xx'}^2} \qquad (9)$$

where: x and x' represent any pair of the phase space coordinates x,x'; y,y'; $\phi,\Delta E/E$; ε_x is the beam rms emittance and N is the number of particles.

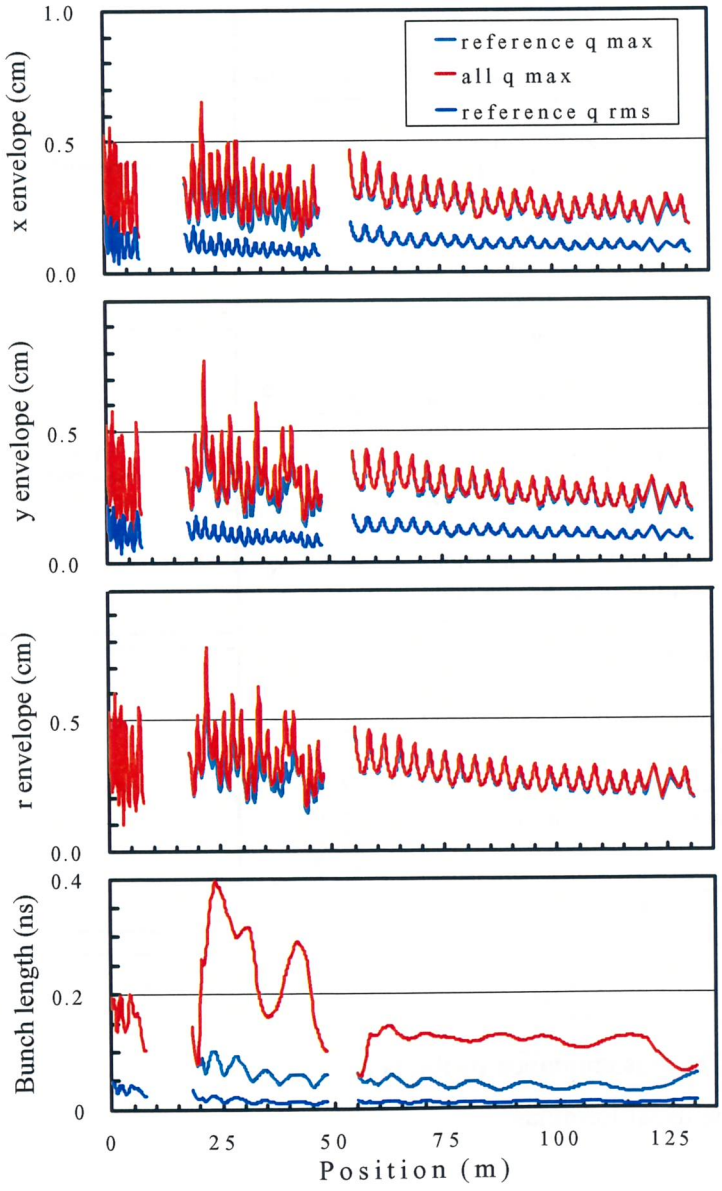

Figure 19: beam envelopes along the three sections of the linac for 4000 ions of ^{132}Sn at a uniform initial distribution and multi-charge beam transport in the "2-strippers" mode.

The reference and the transported charge states (q) are given in table 11. The correlation parameter is defined as $r = \sqrt{(x^2+y^2)}$. The gaps in the plots represent the stripping sections.

The large change in the bunch length after the strippers reflects the separation of the beam in different q-bunches around their synchronous phase.

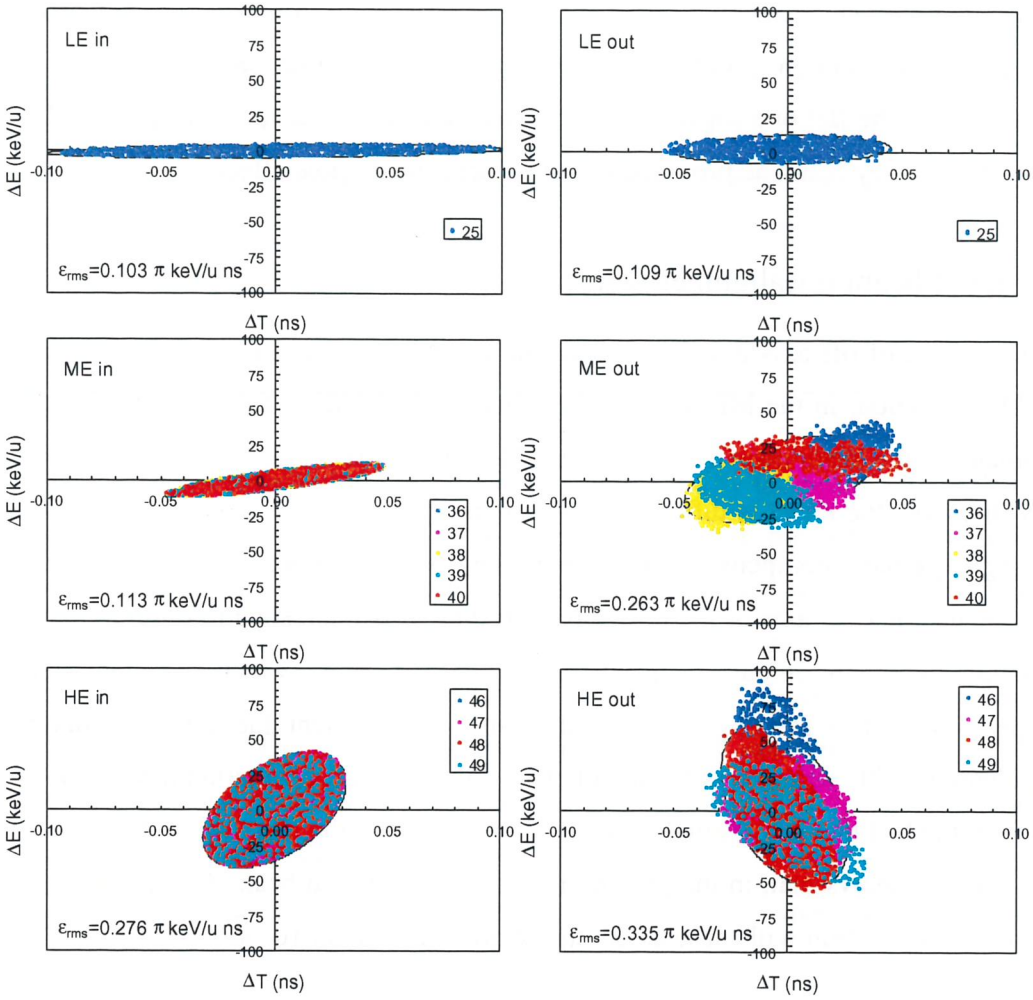

Figure 20: Input and output longitudinal emittance of the three energy sections. Simulation performed with 4000 particles of the test beam ^{132}Sn, transported in the 2-stripper mode of operation and multi-charge beam transport. Each color represents a different charge state. The rms emittance is given in the plots.

As mentioned in the beginning of this section, the larger emittance growth is in the ME section. This could be reduced, if required, by some changes in the design. A multi-charge separation and bunching section could be used after each change of cavity frequency; however, this would result in a cost increase hard to justify. The use of HWR also in the ME section could cancel steering; moreover, with properly shaped inner conductor like the flat one suggested by Delayen *et al.* [46] and adopted by ACCEL [47] for light ions, they could be provided with a reduced quadrupole effect.

6.4 Input beam misalignment effects

The effect of off-axis displacement of the input beam could be tested by means of LANA simulation. In the ME section, the transversal emittance grows proportionally to the square of the beam displacement (figure 21). Due to the presence of QWR steering in the y direction, the effect is different for misalignment in x and y. It is known that QWR steering is partially compensated by rf defocusing if the beam axis is properly displaced from the geometrical axis of the resonator drift tube. It is interesting to observe that ε_x is minimum with an initial x misalignment of 0.4 mm, which denotes steering compensation. The y steering is cancelled by an x displacement due to the x-y mixing of the solenoids (although in this tuning alternate solenoid field orientation have been used) and from the fact that our simulation starts in the middle of the first solenoid.

Figure 21 shows that, in the present design, off-axis initial beam displacement of 0.7 mm in the ME section will cause an emittance growth of about 10 %.

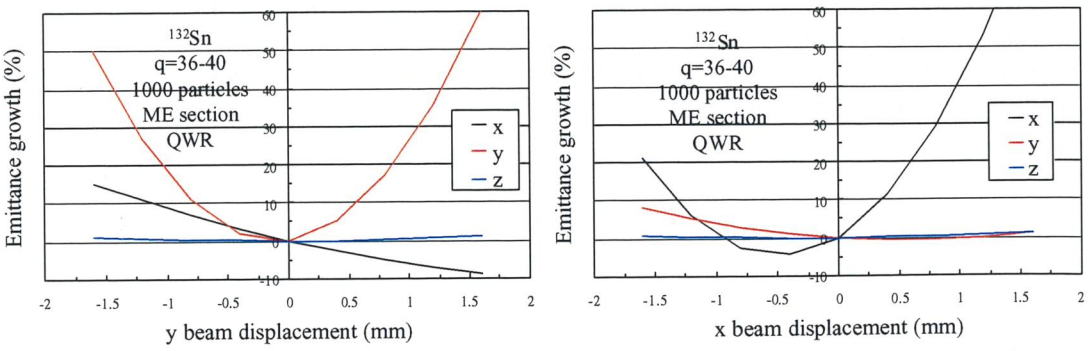

Figure 21: rms emittance growth in the three directions, as function of initial beam displacement in the y (vertical) direction (left) and in the x (horizontal) direction (right).

Other kind of stability tests, like random misalignment of the linac components, RF jitter and loss of some cavities, have not been performed for this lattice yet. Ostroumov studied misalignment in the ANL design of RIA [15]: in the medium energy section (between 9 and 85 MeV/u), he introduced cavities and solenoids with rms misalignment of 0.17 mm, and RF field fluctuations of 0.3 % in phase and 0.3 % in amplitude. He found, in a 5 charges beam transport with ^{238}U beam, a ~20 % transversal emittance growth in both x and y directions and, in the worst case, an emittance growth by a factor 2.4. In the longitudinal phase space the average emittance growth was ~27 % and, in the worst case, a factor of 3.7 [15].

6.5 Beam intensity limitations

The maximum beam current that could be transported by the proposed accelerator is important in the view of a possible use with stable beams, e.g. for in-flight production of radioactive ions. In the "no-stripper" mode, the beam intensity is limited mainly by the RF power system (amplifiers, cables, couplers); in principle, any beam intensity below space charge limit (up to a few mA) could be accelerated by the SRL linac downstream the RFQ resonators. The planned 500 W amplifiers allow beam intensity up to about 300 eμA. This value could be doubled, with minor modification of the cavity RF power-couplers and lines, by using 1 kW amplifiers. For any beam current above approximately 5 μA, normal-conducting RFQs would be required, since the expected 5 % beam losses would not be tolerated by a superconducting structure.

For the operation modes that include strippers, the main concerns are power loss in strippers and beam straggling. The longitudinal and the transversal straggling have been calculated by means of the code SRIM [38] with 10^4, ^{132}Sn particles. The straggling after the second stripper is shown in figure 22. The beam loss due to energy straggling is negligible, but the one caused by transversal straggling may be significant. Assuming a linac acceptance that is 1, 2 or 3 times the nominal beam size, the beam tail originated by transversal straggling cause beam loss of 0.5 %, 0.1 % and 0.05 %, respectively. These straggled particles have a continuous spectrum that is difficult to eliminate and may

activate the entire accelerator. This fact has important consequences when strippers are used in a high beam intensity linac [23].

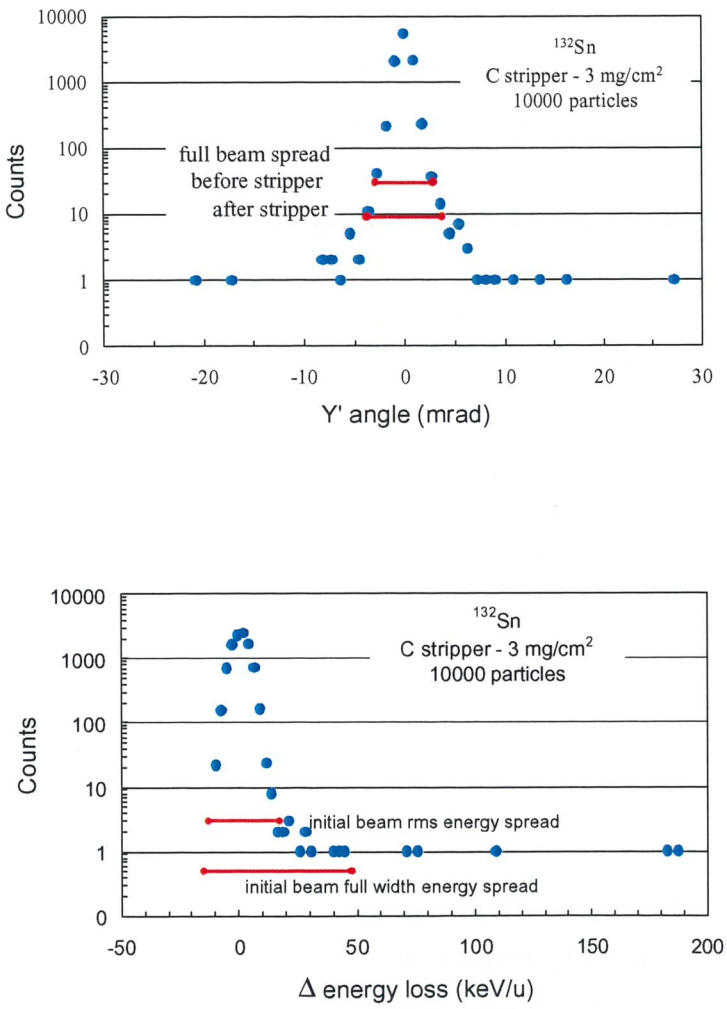

Figure 22: energy and angular straggling simulated using SRIM for the EURISOL second stripper. The blue points represent the stripper contribution only. Top: angular straggling. The upper red line represents the rms angular spread of the multi-charge beam before the stripper; the lower red line represents the rms angular spread of the multi-charge beam after the stripper, calculated by quadric sum of the initial beam rms spread and the rms straggling caused by the stripper. Bottom: energy straggling. The upper red line represents the rms energy spread of the multi-charge beam before the stripper; the lower red line represents the rms energy spread of the multi-charge beam after the stripper, calculated by quadric sum of the initial beam rms spread and the rms straggling caused by the stripper.

6.6 Design in the absence of multi-charge bending section

In the proposed EURISOL post-accelerators, achromatic and isochronous bending sections are required to extract the multi-charge beam to the intermediate experimental areas, and to clean the beam from unwanted particles. Three main types of multi-charge bending sections have been suggested: S-bend [26,28], U-bend [26] and Ω-bend [27]. These bending sections, still under theoretical study, are rather complex and expensive. Moreover, their reported Δq/q acceptance values of ±2.5 % [26] and ±5 % [28] are not sufficient for 5-charge bending in the ME section of the EURISOL post-accelerator.

A linac design without bending sections was then considered (figure 23).

The main advantages of such a configuration, in comparison with the standard one, are:

1. Construction cost savings,
2. Higher transmission.

The main drawbacks are:

1. Lower beam quality,
2. Loss of isotope and isobars discrimination power.

In this revised scheme, after stripping, the charge states that exceed the linac acceptance are lost along the accelerator. Since the beam intensity is very low, these losses are expected to cause tolerable activation.

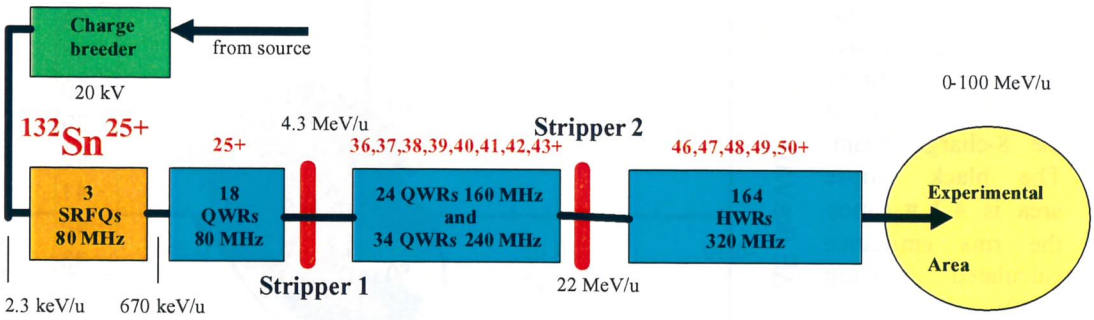

Fig 23: Revised schematic layout of a post-accelerator linac without multi-charge bending sections (see fig.1 for comparison).

In order to study this scheme, we performed beam dynamics simulation with 8 charges, q=36-43, created by the first stripper and transported through the ME section. The simulation results, compared to the previous configuration (with bending sections),

are shown in table 12. In this simulation, charge state 37 was still used as the reference charge and the transversal tuning developed for the standard 5-charge states transport has been kept. The somehow lower output energy is due to the gradient, lower than in the standard case, required at the end of the ME section to collect all q-bunches together.

Table 12: Simulation results of 8-charges transported through the ME section. Simulation performed with 4000 particles of ^{132}Sn. 21 particles (~0.5 %) lost. The input parameters are the usual ones. The right column is the ratio between the results obtained transporting 8- and 5-charge states.

	8-charge	8-charge/5-charge
q	36-43	
Stripper efficiency	95.3 (%)	1.23
Total transmission	94.8 (%)	1.22
Acceptance $\pm\Delta q/q$	~10 (%)	1.6
Output energy	21.7 (MeV/u)	0.97
ε_x	0.251 (π mm mrad)	1.6
ε_y	0.198 (π mm mrad)	1.5
ε_z	0.775 (π keV/u ns)	2.9

The main effect on the beam quality is the longitudinal emittance growth. The output longitudinal phase space is presented in figure 24. Most of the lost particles belong to charge state 43. In the absence of bending sections, a $\Delta q/q=\pm 10\%$ acceptance can be obtained.

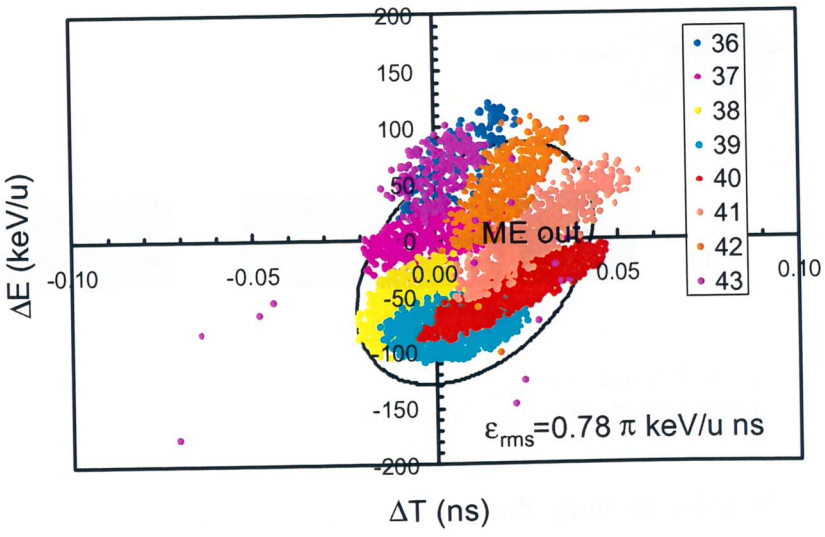

Figure 24: longitudinal phase space, at the exit of the ME section, of the 8-charge beam. The black ellipse area is 4.2 π times the rms emittance calculated using eq.(9).

The larger q acceptance (fig. 23) could allow the use of a thin foil as second stripper. This produces lower average charge state (thus lower acceleration efficiency), wider charge distribution (thus difficulties in charge collection and transport) but, on the other hand, this reduces straggling and emittance growth. In a thick foil the transverse emittance growth (table 7) is in the order of the growth due to 8-charges transport. Thin foils allow, if required, more intense beam than thick ones [23].

The overall advantages of the straight configuration, however do not seem to be significant. The estimated construction cost of the bending sections is less than 5 % of the total linac. It might be useful to design the linac with the two options coupled together, a Ω bending section for higher beam quality and a straight shortcut for higher transmission and faster set-up.

7 Conclusion

The preliminary beam dynamics simulations of the SRL linac have shown that, in the proposed configuration, the final beam quality is very good in the no-stripper mode of operation, where most of the experiments are expected, and still satisfactory in the 1- and in the 2-stripper mode of operation, which allows the particles reaching the maximum energy. The multicharge beam transport after stripping allows a significant reduction of the linac size, while maintaining high transmission efficiency; multicharge bunching/debunching allow keeping the longitudinal emittance within acceptable limits.

To complete and fortify the proposed solution additional study is needed: component misalignment and RF jitter; full simulation in the three mode of operations and the three test case beam ^{33}Ar, ^{132}Sn and ^{210}Fr; detailed study of the multi-charge bending section after each stripper; different scenarios, e.g. in the absence of very high charge breeding.

A linac scheme like the one proposed in this work can reach the EURISOL post-accelerator requirements.

8 Appendix 1: updating of our previous EPAC2002 paper

The current document has been written during July 2002 after the acceptance for publication of our paper submitted to the EPAC 2002 [5]. After double-checking and refine of the calculation some numbers in the above paper should be updated. To make it clear the correct numbers are summarized below:

1. In figure 1 of ref. [5] the SRFQ section should be about 4 m long.
2. In section 3 of ref. [5] the q/A acceptance should be ±6.6 %.
3. In section 3 of [5] should be written, "The transversal emittance … 10 % growth for a 0.7 mm off-axis initial displacement …"
4. In section 3 of ref. [5], according to our recent calculation, correct to; "Assuming a linac acceptance that is 3 times … straggling will cause a 0.05 % beam loss."

9 Acknowledgments

This work was performed in the framework of the EURISOL collaboration and took advantage of the studies performed for the RIA and ISAC-II projects, in which we have been partially involved. We wish to thank D. Gorelov (MSU-NSCL) for giving us the beam dynamics simulation code LANA and for the precious discussions and suggestions on multicharge beam dynamics in RIA; A. Pisent and M. Comunian (LNL), for fruitful discussion on beam dynamics problems and for continuous help in our work; V. Zviagintsev (LNL) for performing all calculations of realistic fields in superconducting resonators; M. Pasini and B. Laxdal (TRIUMF) for the very useful discussions on multicharge beam dynamics of ISAC-II.

We are grateful also to Iris Berkovits, who performed the calculations on stripper effects with the SRIM code.

10 References

[1] EURISOL – *"The European Isotope Separation On-Line Radioactive Nuclear Beam Facility"*, http://www.ganil.fr/eurisol/ .

[2] M-H Moscatello, *"Post-Accelerators and Mass-Separators For EURISOL"*, Second EURISOL town meeting, Abano Terme, 24-25/01/2002, http://www.ganil.fr/eurisol/TOWN_MEETING_ABANO/Moscatello.pdf.

[3] B. Launé *et al.*, *"Post-Accelerator and Mass-Separator Group Cyclotron Options"*, Second EURISOL town meeting, Abano Terme, 24-25/01/2002, http://www.ganil.fr/eurisol/TOWN_MEETING_ABANO/BernardLaun%e9.pdf.

[4] A. Facco, *"Linac option for post-accelerator"*, Second EURISOL town meeting, Abano Terme, 24-25/01/2002, http://www.ganil.fr/eurisol/2ndTM-Programme.html.

[5] D. Berkovits, A. Facco, M. Comunian, Z. Lipeng, A. Pisent, F. Scarpa and V. Zviagintsev, *"Studies on a 100 MeV/u superconducting post-accelerator linac for EURISOL"*, accepted for publication in the Proc. of EPAC2002, June 3-7, Paris (2002).

[6] A. Facco and V. Zviagintsev, *"Completion of the LNL Bulk Niobium Low Beta Quarter Wave Resonators"*, Proc. of 9th Workshop on RF Superconductivity, Santa Fe, Nov. 1-5, (1999)203.

[7] P. N. Ostroumov and K. W. Shepard, *"Multi-charge beam dynamics in an ion linac"*, Phys. Rev. ST-AB 3(2000)030101.

[8] P. N. Ostroumov, R. C. Pardo, G. P. Zinkann, K. W. Shepard and J. A. Nolen, Procceedings of LINAC 2000, Monterey, California, 21-25 August 2000, MOD02 and *"Simultaneous Acceleration of Multi Charged Ions through a Superconducting Linac"*, Phys. Rev. Lett. 86(2001)2798.

[9] A. Facco and V. Zviagintsev, "Study on beam steering in intermediate-β superconducting quarter wave resonators", Proc. of PAC2001, Chicago, June 18-22, (2001)1095.

[10] P. N. Ostroumov and K. W. Shepard, *"Correction of beam-steering effects in low-velocity superconducting cavities"*, Phys. Rev. ST-AB 4(2001)110101.

[11] A. Facco and V. Zviagintsev, *"Beam steering in low-β superconducting quarter wave resonator"*, LNL-INFN Annual report (2001)250 and *"Study on beam steering in intermediate-β superconducting quarter wave resonators"*, LNL-INFN Annual report (2001)252. Available at http://www.lnl.infn.it/index.html.

[12] W. Bräutigam, O. Felden, M. Glende, H. Jungwirth, A. Lehrach, R. Maier, S. Martin, A. Schnase, Y. Senichev, R. Stassen, R. Tölle, E. Zaplatin, A. Facco and V. Zviagintsev, "*SC ACCELERATOR COMPONENTS FOR LIGHT ION LINACS*", SRF2001, Tsukuba, Japan, September 6-11 (2001).

[13] D. V. Gorelov and P. N. Ostroumov, *"Application of LANA code for design of Ion Linac"*, EPAC96, Sitges, Spain, June 10-14, (1996)1271.

[14] D. Gorelov, MSU, LANA code versions 9.1.7 to 9.4.8 and attached examples, privet communication (2001-2002), gorelov@nscl.msu.edu.

[15] P. N. Ostroumov, *"Development of a medium-energy superconducting heavy-ion linac"*, Phys. Rev. ST-AB 5(2002)030101.

[16] D. Gorelov, J. Kim, F. Marti, H. Podlech, X. Wu and R. York, *"Superconducting driver linac beam dynamics optimisation for RIA"*, Proc. of PAC2001, Chicago, June 18-22, (2001)4086.

[17] J. Kim, D. Gorelov, F. Marti, H. Podlech, X. Wu and R. York, *"Design study of a superconducting linac for RIA"*, Proc. of PAC2001, Chicago, June 18-22, (2001)1741.

[18] D. Gorelov, T. L. Grimm, W. Hartung, F. Marti, H. Podlech, X. Wu and R.C. York, *"Beam Dynamics Studies at NSCL of the RIA Superconducting Driver Linac"*, accepted for publication in the Proc. of EPAC2002, June 3-7, Paris (2002).

[19] M. Pasini and R. Laxdal, *"Beam Dynamics Studies on the ISAC-II Post-Accelerator at TRIUMF"*, accepted for publication in the Proc. of EPAC2002, June 3-7, Paris (2002).

[20] R. E. Laxdal and M. Pasini, *"ISAC-II optics specifications"*, TRI-DN-01-xx, April 12 (2002), available at http://www.triumf.ca/download/lax/ISAC5.ps .

[21] M. Pasini and R. E. Laxdal, *"ISAC II: Beam studies with multi-charge beams"*, TRI-DN-01-08, April 9, (2001), available at

http://www.triumf.ca/download/lax/multicharge_note.pdf.

[22] Y. Blumenfeld , *"Reaction studies"*, Second EURISOL town meeting, Abano Terme, 24-25/01/2002, http://www.ganil.fr/eurisol/TOWN_MEETING_ABANO/YorickBlumenfeld.pdf.

[23] D. Berkovits and A. Facco, *"Stripping effects in a heavy ion LINAC accelerator"*, LNL report no. LNL-INFN (REP) 191/2002 (2002)1-32.

[24] A. Pisent et al., *"The new LNL injector PIAVE based on a superconducting RFQ"*, Proc. of EPAC98, Stockholm, June 22-26 (1998)758.

[25] H. Podlech, D. Gorelov, J.-W. Kim, F. Marti and R. York, *"An injector for a multi ion beam driver linac"*, Proc. of PAC2001, Chicago, June 18-22, (2001)3933.

[26] M. Portillo, V. N. Aseev, J. A. Nolen and P. N. Ostroumov, *"Design of a magnetic optical system for transport and matching of multiple-charge state heavy ion beams"*, Proc. of PAC2001, Chicago, June 18-22, (2001)3012.

[27] X. Wu, D. Gorelov, T.L. Grimm, W. Hartung, F. Marti, H. Podlech and R.C. York, *"The Design of the Isochronous and Achromatic Charge-Stripping Sections for RIA"*, accepted for publication in the Proc. of EPAC2002, June 3-7, Paris (2002).

[28] M. Pasini and R. Laxdal, *"An Isopath Achromatic Bending Section for Multi-charge Ion Beam Transport at ISAC-II"*, accepted for publication in the Proc. of EPAC2002, June 3-7, Paris (2002).

[29] T. Wangler, *"RF Linear Accelerators"*, John Wiley & Sons, NY 1998.

[30] R. Pardo, ANL, privet communication 1992-1998, based on Y. Baudinet-Robinet, *"Equilibrium charge-state distribution of highly stripped ions in carbon foils"*, Nucl. Instr. and Method 190(1981)197-202.

[31] A. Leon *et al., "Charge state distribution of swift heavy ions behind various solid targets"*, At. Data and Nucl. Data Tables 69(1998)217-238.

[32] W. Kutschera, I. Ahmad, B. G. Glagola, R. C. Pardo, K. E. Rehm, D. Berkovits, M. Paul, J. R. Arnold and K. Nishiizumi, *"Accelerator mass spectrometry of ^{59}Ni in extraterrestrial matter"*, Nuclear Instruments and Methods in Physics Research B 73(1993)403-412.

[33] R. O. Sayer, Revue de Physique Appliquee, 12(1977)1543.

[34] T. Lamy *et al.*, *"The Development of the ECRIS Charge State Breeder for Generating RIB's"*, Proc. of CAARI2000, Denton, In the proceedings of AIP April 2001 and P. Sortais *et al.*, *"ECR Ion Source as Charge Breeder of Radioactive Ions"*, International Workshop on Production of Radioactive Ion beams, Feb. 12-17, Puri, INDIA (2001).

[35] P. N. Ostroumov, J. A. Nolen, Jr., R. C. Pardo and K. W. Shepard, *"Design of a post accelerator for the rare isotope accelerator facility"*, Proc. of PAC2001, Chicago, June 18-22, (2001)4080.

[36] ANSOFT, HFSS-8, http://www.ansoft.com/ (2001).

[37] H. Ernst, IRMA code, ANL, 1981.

[38] J. F. Ziegler and J. P. Biersack, SRIM code, http://www.srim.org/ (2000).

[39] J. F. Ziegler, *"The Stopping of Energetic Light Ions in Elemental Matter"*, J. Appl. Phys. Rev. Appl. Phys., 85(1999)1249-1272.

[40] N. Catalan Lasheras, M. Crescentr and m. Vretenar, Proc. of LINAC96, Geneva, Switzerland, August 26–30, 1996, TUP17.

[41] W. Barth, et al., *"High Current Transport and Acceleration at the Upgraded UNILAC"*, Linac98, Chicago, U.S.A., (1998)454.

[42] W. Barth, L. Dahl, J. Glatz and J. Klabunde, *"Beam measurements at the GSI high current injector"*, Proc. of PAC2001, Chicago, June 18-22 (2001)3281.

[43] J. Glatz, B. Langenbeck, *"A High Duty Foil Stripper System in the Injection Line to the Heavy Ion Synchrotron SIS at GSI"*, Proc. of EPAC96, Sitges (Barcelona), May 10-14 (1996) 2406.

[44] American Magnetic, Oak Ridge, TN, (2002), http://www.americanmagnetics.com/magnets/highsol.html .

[45] Nicolas Pichoff, ESS-European Spallation Source, August 27-28 (2001), http://web.concert.free.fr/workshops/AugustSaclayBrainstorming/NPichoff-Beamdynamics.pdf.

[46] J. R. Delayen, C. L. Bohn, C. T. Roche, *"Experimental Results in Superconducting Niobium Resonators for High-Brightness Ion-Beam Acceleration"*, Proc. of the 1990 Linear Accelerator Conference, Albuquerque, New Mexico, 10-14 Sept. 1990, Los

Alamos Report LA-12004-C, 85-87 (1991) and *"Application of RF Superconductivity to High-Brightness Ion Beams Accelerators"*, Los Alamos Report LA-12004-C, 82-84 (1991) and Nuclear Instruments and Methods in Physics Research, B56/57, 1025-1028 (1991).

[47] M. Pekeler, K. Dunkel, C. Piel, H. Vogel and P. vom Stein, *"Design of a 40 MeV Linear Accelerator for Protons and Deuterons using Superconducting Half Wave Resonators"*, Proc. of EPAC2002, June 3-7, Paris (2002).